UNIVERSITY OF OKLAHOMA

GRADUATE COLLEGE

NOVEL TARGETED ANNEXIN V - DRUG CONJUGATE FOR CANCER CHEMOTHERAPEUTIC TREATMENT

A THESIS

SUBMITTED TO THE GRADUATE FACULTY

in partial fulfillment of the requirements for the Degree of

Master of Science

By

BENJAMIN MARK SOUTHARD

Norman, Oklahoma

2019

NOVEL TARGETED ANNEXIN V - DRUG CONJUGATE FOR CANCER CHEMOTHERAPEUTIC TREATMENT

A THESIS APPROVED FOR THE

STEPHENSON SCHOOL OF BIOMEDICAL ENGINEERING

BY

Dr. Roger Harrison, Chair

Dr. Vassilios Sikavitsas

Dr. Matthias Nollert

Acknowledgements

I would like to thank my committee, Dr. Matthias U. Nollert, Dr. Vassilios Sikavitsas, and Dr. Roger Harrison for their guidance and willingness to help throughout both course work and lab work. I am especially grateful to Dr. Harrison for his mentorship which began more than 4 years ago when he allowed me to participate in his laboratory group as I was entering my second year at OU. The opportunities, advice, and insight that you have provided me have set me up for success wherever life takes me.

I would also like to thank the funding sources that have helped to make this research possible: Gallogly College of Engineering, Peggy and Charles Stephenson School of Biomedical Engineering, School of Chemical, Biological and Materials Engineering, University of Oklahoma Institute for Biomedical Engineering, and the Jean Wheeler Sparks and Baxter Abbott Sparks Breast Cancer Research Fund at the OU Foundation.

I am so grateful to my former colleagues in Dr. Harrison's group, Patrick McKernan and Needa Virani, who taught me not only to perform but to understand everything from cell culture to flow cytometry to conjugation chemistry. I would also like to thank all the faculty, staff, and graduate students who have been part of the Biomedical Engineering and the Chemical, Biological, and Materials Engineering departments during my time here, specifically: Cherie

Hudson, Nancy Cotter, Shayla Glover, Madena McGinnis, Donna King, Terri Coliver, Dr. Lei Ding, Dr. Edgar O'Rear, Dr. Daniel Resasco, Michael Felder, Sabrina Garner, Charles Bagarie, and my current labmates Alexis Woodward and Gabrielle Faria.

I also need to recognize my friends and family who have selflessly supported me mentally, emotionally, and sometimes physically. Thank you, Kyle Smith, Suparsh Parikh, and Nathan Bugg for always having open hearts and ears. Thank you, Eamon (my dog) for never failing to cheer me up. Thank you, Avery Rich for being a constant companion and coconspirator. And finally, the greatest thank you goes to my family: my parents Mark and Laura Southard, my sisters Carol and Katie, and my brother Bill. Thank you for always encouraging, challenging, and most of all loving me. My achievements are due to all the names listed here and to all of them, thank you.

Table of Contents

Abstract

Annexin V-DM1 is a protein-drug conjugate that is designed to deliver the covalently linked DM1 cytotoxic payload to tumor cells. The drug is a potent microtubule inhibitor that has been shown to have profound antineoplastic activity at extremely low concentrations by causing mitotic arrest and subsequent apoptosis. The protein binds with high specificity to phosphatidylserine, a phospholipid internally expressed on most healthy cells that is expressed externally in tumor cells. The conjugate was synthesized using a non-cleavable linker and characterized. The average drug to protein ratio was found to be 8. The cytotoxic activity was investigated in vitro using three breast cancer and two leukemia cell lines. The EC50 for EMT6 cells was 0.21 nM for the AV-DM1 conjugate, an increase in effectivity of 130x when compared to unconjugated DM1; for 4T1 cells the EC50 was 0.85 nM, an increase in effectivity of 377x; for MCF7 cells the EC50 was 0.52 nM, an increase in effectivity of 910x; for P388 cells the EC50 was 1.2 nM for the AV-DM1 conjugate, an increase in effectivity of 221x; and for L1210 cells the EC50 was 0.26 nM, an increase in effectivity of 354x.

Chapter I: Introduction

Cancer

Human cancers are the result of a handful of mutations that randomly occur out of hundreds and potentially thousands of proto-oncogenes. The specific molecular phenotypes of these tumors make nearly all patients' cancers unique in clinically profound ways. However, all cancers by their nature share some common attributes such as unbounded growth and proliferation, failure to undergo apoptosis, signaling for angiogenesis, and eventual metastasis [1].

Uncontrolled growth of tumors is usually due to a reduction in or even silencing of key growth suppression genes or growth factor receptor genes like EGFR. However, uncontrolled proliferation can't be sustained indefinitely due to telomere shortening in normal cells. In order to be capable of truly unbounded growth, cancerous cells must have some way to upregulate telomerase activity to avoid eventual apoptosis. Another essential factor to the formation of macroscopic solid tumors is angiogenesis. Promotion of increased vascularity to the tumor microenvironment is crucial to maintaining growth as the tumor margins expand [2-5]

Tumor metastasis is by far the main cause of mortality from cancer. It requires several things to occur but mainly involves a physical translocation of tumor cells

through the blood to a distant location and adaptation of the tumor cells to grow in the new microenvironment. Preparing to migrate is not a trivial task for cancer cells, however. The cells must first shift to a semi-pluripotent state where they can reduce proliferation temporarily, exchange receptors that promote cell-cell binding for receptors that encourage cell movement, and secrete proteases to degrade the local extracellular matrix and allow the exit, then the cells must reverse all of those changes to return to a principally proliferative state in their new location. Many of the factors surrounding how fast growing and easily metastasizing a particular tumor is are influenced by the tissue type from which the cancer originated. This thesis will focus on metastatic breast cancer as well as leukemia [6, 7].

Targeting

Phosphatidylserine

Among all the many and varied biomarkers of cancers, phosphatidylserine (PS) is one of the most ubiquitous, present in nearly all types of cancers including lymphoma, leukemia, lung carcinoma, colorectal carcinoma, melanoma, bladder carcinoma, and breast carcinoma [8].

Comprising up to 15% of the lipid bilayer, PS is expressed in all mammalian plasma membranes, though it is found only on the inner leaflet in the vast

majority of healthy cells. This asymmetry in PS expression is believed to be maintained by a highly selective magnesium and ATP dependent translocase enzyme. Under many conditions representative of both healthy and stressed cells such as aging, migration, viral infection, and most commonly apoptosis, the phospholipid distribution of the membrane is disrupted by a combination of translocase inhibition and calcium dependent phospholipid scramblase upregulation [9-12].

Once expressed, PS plays multiple signaling roles for the immune system. Apoptosis is a mechanism for cell death and debris clearance that avoids an inflammatory response from T and B cells. PS on apoptotic cells is a ligand for macrophages, promoting the migration to and engulfing of the stressed cell by the macrophage. However, tumor cells, especially tumor endothelium, have adopted this false-apoptotic signaling to avoid further investigation by the immune system. While expressing PS that encourages macrophagic endocytosis, they also express surface proteins such as CD47 and CD31 which discourage macrophages from interacting with healthy cells, resulting in pathogenic tissue that pacifies phagocytic cells while suppressing recognition by other immune cell populations [13, 14].

When tumors grow to be greater than 2 mm they must promote a high degree of vascularization to supply sufficient oxygen to the tumor tissue for sustained growth resulting in sprawling and disorganized endothelium overexpressing PS in

macroscopic tumors [15, 16]. Tumor vasculature forms in a rapid and random manner. The immature endothelium fails to make the same tight cell-cell junctions found in regular blood vessels; where normal endothelium is essentially impermeable to particles greater than 2 nm, the spaces between cells in tumor vasculature can range from just a few nanometers to micrometer or larger gaps, greatly increasing the permeability and penetration of particles into the tumor tissue. The disorganized nature of tumor vasculature has been well documented as the enhanced permeability and retention (EPR) effect [17, 18]. This combination of factors makes PS an ideal ligand for tumor-targeting drug delivery strategies.

Annexin V

Annexin V (AV) is a protein from a family of calcium-dependent, membrane-binding proteins. In the body naturally, it acts as a powerful anticoagulant, coating cell surfaces and preventing membrane-membrane adhesions. It is comprised of an amphipathic monomer that contains four domains that create a central convexity that strongly associates with phosphatidylserine exposed on the surface of cells in the presence of calcium (KD < .2 nM). It is suspected that the presence of zinc can increase the affinity of AV for PS [19, 20].

AV is a monomer in solution, but it has the ability to form trimer crystals with other AV proteins through associations between domain one of one protein and domain three of another. These trimers can also associate with other trimers,

creating a two dimensional lattice of the surface of cells. This puts pressure on the cell membrane as the lattice retains the convex shape of the individual AV monomers, inducing endocytosis of the PS-expressing/AV-bound portions of the cell membrane as shown in Figure 1 [21, 22].

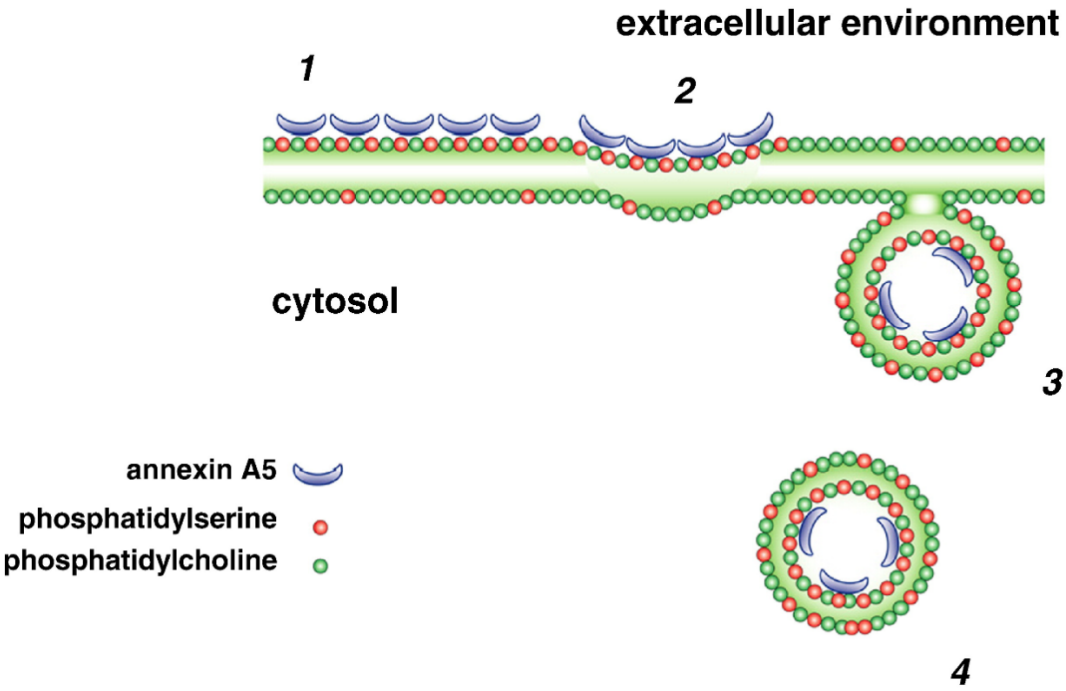

Figure 1. Annexin binding and endocytosis [21].

Mertansine

Historical Background

In December of 1971, President Nixon signed into law the National Cancer Act, declaring a "war on cancer". This act empowered the National Cancer Institute and appropriated hundreds of millions of dollars over the next few years to establish the first 15 national cancer centers around the country and support research to "conquer cancer" [23, 24].

One of the immediate products of this unprecedented initiative was the discovery of a class of molecules termed "maytansinoids". In 1972, Kupchan published the first paper describing the isolation, structure, and antileukemic activity of what he called an "ansa macrolide" from the *Maytenus serrata* plant, a short, shrub-like tree from central Africa [25, 26]. Kupchan expanded upon his findings two years later, describing four more maytansinoid derivatives and their profound activity against B16 melanoma and lung carcinoma cell lines [27].

By 1975, other labs had begun to take an interest in the antineoplastic potential of the maytansinoids, and the mechanism of action had begun to be elucidated. M phase mitotic arrest and cross-resistance to vinca alkaloids were indicative of microtubule inhibition [28-30]. By 1978, the first Phase 1 clinical trials of maytansine had shown fantastic results with leukemia, with several patients going

into complete remission and patients that had been treated with and were resistant to vincristine, another microtubule inhibiting agent, showed marked improvement. Trials with breast cancer and melanoma were not as encouraging. Unfortunately, maytansine showed significant gastrointestinal and central nervous system toxicity. Severe vomiting and diarrhea were nearly universal reactions to the drug; lethargy, weakness, and insomnia were also commonly reported. The combination of these adverse toxicities resulted in some patients refusing to continue treatment with maytansine [31-33].

Most of the excitement surrounding maytansinoids had passed by the early 1980s due to disappointing therapeutic results at the maximal tolerated doses in clinical trials which was only around 1 mg/m^2 [34]. With the advent of humanized monoclonal antibodies in 1988 and the subsequent flurry of research surrounding immunoconjugates, maytansinoids were given a second look by Goldmacher. In order to increase the therapeutic index of highly potent drugs like maytansine, he began make modifications to the molecule to make it easier to link to monoclonal antibodies. The first of the modifications was to introduce a sulfhydryl group to the molecule in order to allow a disulfide bridge to be made between drug and protein. This modified maytansinoid became known as “drug maytansinoid-1” or DM1, which showed 3-10x more antitumor activity than maytansine. Clinical trials on antibody conjugated maytansinoids began as early as 2002 with antibodies like anti-NCAM1 and cantuzumab for colorectal, pancreatic, lung and myeloma cancers, TA.1-DM1 for HER2+ breast cancer, C242-DM1 for colorectal

and pancreatic, N901-DM1 for small cell lung cancer, and J591-DM1 for prostate cancer [35].

These trials as well as pre-clinical work showed maximal tolerated weekly doses of 115 mg/m^2, over 100 times the dose possible with the unconjugated drug, and reduced toxicity by 1000 times to non-antigen presenting cells [36-38]. Since then, much more work has been done in characterizing and elucidating the specific mechanisms of maytansine derivative conjugates. In 2013, trastuzumab-DM1, trade name Kadcyla, was the third ever antibody drug conjugate to receive FDA approval in the United States. It is approved to treat HER2 positive metastatic breast cancers and is undergoing more clinical trials to investigate possible drug combinations [39]. Other drugs currently in clinical trials include lorvotuzumab mertansine for recurrent neuroblastomas and bivatuzumab mertansine for CD44v6 positive breast cancer [40, 41].

Mechanism of Action

Mertansine (drug maytansinoid 1, DM1) is a microtubule inhibiting agent with an easily accessible sulfhydryl group which can be conjugated to proteins in a variety of both cleavable and non-cleavable linkages. Its structure is shown in Figure 2.

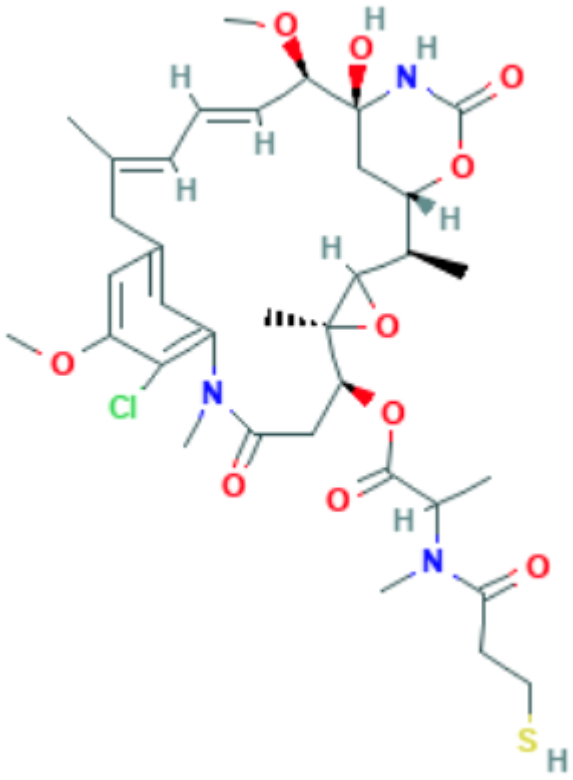

Figure 2. Mertansine Chemical Structure, Formula: $C_{35}H_{48}ClN_3O_{10}S$ [42].

It has a molecular weight of 738.3 Da. It is sparingly soluble in aqueous solutions and is soluble in DMSO up to about 10 mM [43]. It was originally thought that maytansinoids acted on the same site on tubulin as vinca alkaloids because they appear to competitively inhibit each other and binding is mutually exclusive. It is now suspected that mertansine binds to tubulin in a distinct site entirely on the beta-tubulin domain preventing longitudinal microtubule assembly in contrast to vinblastine and the other vinca alkaloids that bind in between the alpha- and beta-tubulin heterodimers, acting as a sort of wedge, causing useless curved microtubules to form as shown in Figure 3. Regardless of the separate binding

sites, the formation of one drug-tubulin complex causes the occlusion of the other site. Mertansine's dissociation constant (K_D) for beta-tubulin is about 1 uM, a 20x stronger affinity for binding sites than vinblastine [44-46].

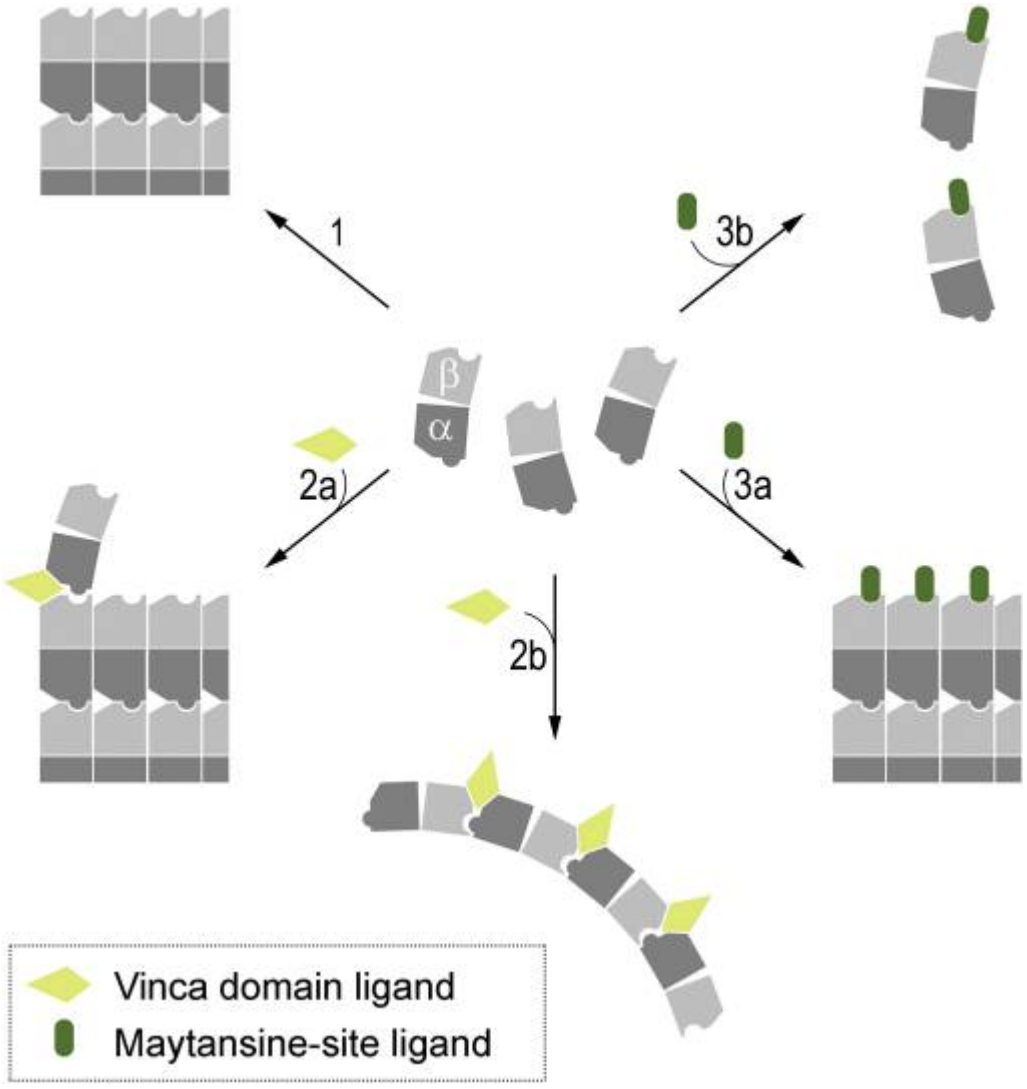

Figure 3. Mertansine tubulin binding interaction and inhibition [47]. Step 1 indicates uninhibited microtubule polymerization, 2a and b show the binding site and the resulting crooked microtubules of vinca alkaloids. 3a and b show the maytansinoid binding site and inhibition of longitudinal polymerization.

Microtubule inhibition results in metaphase mitotic arrest as the mitotic spindle is unable to attach to all chromosomes in order to pull them apart. Prolonged time in mitotic arrest generally results in DNA damage, apoptosis, and unviable daughter cells with unusual numbers of chromosomes due to a failure of spindle segregation. As the cell remains in metaphase, cyclin B1 phosphorylates the anti-apoptotic protein Mcl-1 leading to its degradation and the upregulation of caspase enzymes that begin to attack critical cell components. Mitosis also exposes the telomeres of the chromosomes to damage from caspase and cytosolic DNases causing a strong DNA damage reaction from the cell, further upregulating apoptotic enzymes and cofactors [48].

Cleavable linkers like N-succinimidyl 4-(2-pyridyldithio)butanoate (SPDB) generally form a reducible disulfide bond between the protein and the drug. In extracellular environments, the disulfide bond is stable and the drug is not released, but the intracellular environment is much more easily reduces the disulfide bond, releasing the drug once it has been internalized. Non-cleavable linkers like succinimidyl 4-(N-maleimidomethyl)cyclohexane-1-carboxylate (SMCC) require digestion by lysosomes in the cell before the drug is released. A structural comparison of cleavable vs. non-cleavable linkers can be found in Figure 4. Metabolites of the non-cleavable linker and drug combination mAb-SMCC-DM1 have shown to be at least as effective as the parent molecule, the vast majority of which are S-Methyl-DM1 and lysine-SMCC-DM1 [49-51]. Now that drug conjugates are possible, DM1 makes an exceptionally attractive and

potent option for antibody linkages with its solitary thiol group. An amine-to-sulfhydryl crosslinker like sulfo-SMCC could easily link the active drug molecules to lysine residues in AV.

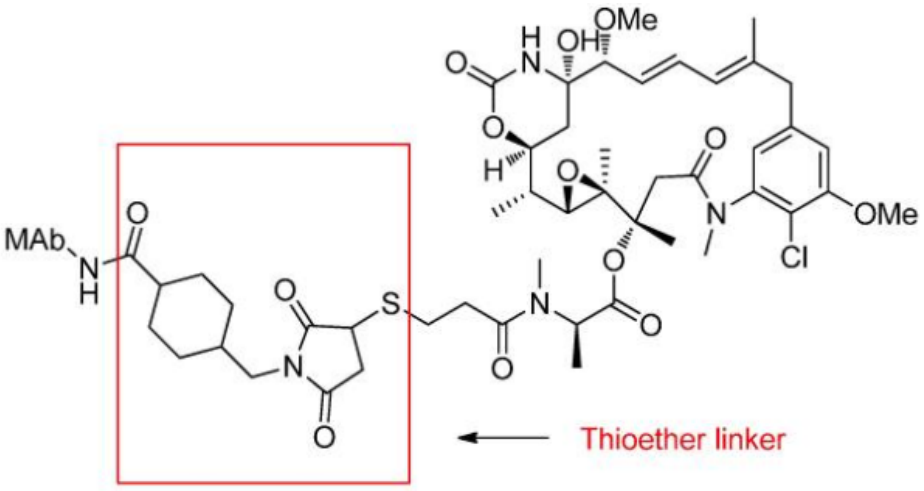

MAb-SMCC-DM1

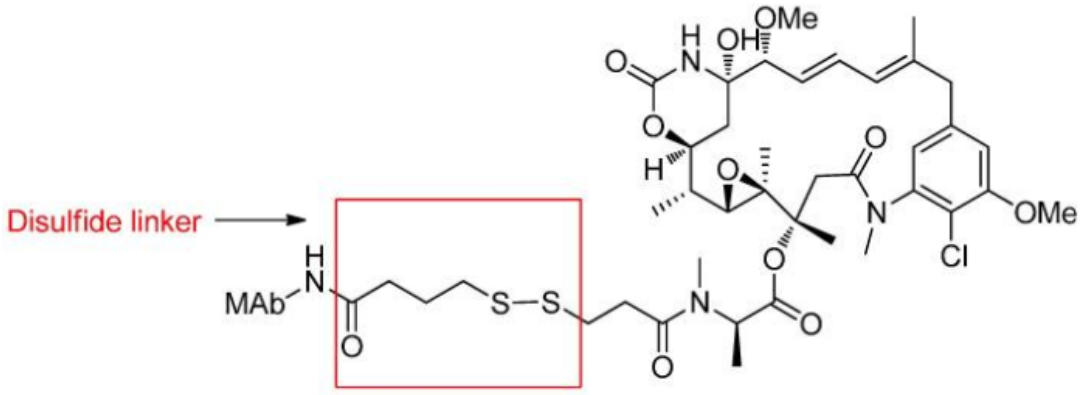

Cantuzumab mertansine

Figure 4. Different linkers allow different types of cleavage chemistry. Thioether linkages require digestion by proteases in lysosomes. Disulfide linkages may be reduced in the intracellular space, but remain stable in the plasma [52].

Scope of Thesis

Traditional chemotherapies are limited by wide ranging adverse effects on various unintended targets such as the nervous system, immune system, and gastrointestinal tract. Efficacy of these drugs is throttled by the need to reduce their systemic toxicity by lowering the overall dose. Antibody-drug conjugates attempt to overcome this obstacle by providing a vehicle to circulate in the plasma that will only release the active drug molecules once they are bound to tumor specific antigens. However, antibody-drug conjugates can be vulnerable to rapidly changing tumor phenotypes and low antigen expression in most tumor strains. This narrows the utility of these conjugates by increasing the cost of these treatments while reducing their applicability.

This thesis is focused on the synthesis, characterization, and preliminary evaluation of the antineoplastic activity of a small protein-drug conjugate that targets a ubiquitous and specific marker of tumor vasculature with a non-cleavably linked, highly potent drug molecule to maximize tumor inhibition while minimizing systemic toxicity.

Chapter II: Materials and Methods

Materials

The pET-30 Ek/LIC/ANXA5 plasmid was constructed and sequenced by Oklahoma Medical Research Foundation as previously described [53].
The 5 mL HisTrap chromatography column was purchased from GE (Boston, MA). HRV 3C protease was purchased from Novagen (Madison, WI). Bradford reagent, SDS-PAGE gels, Imperial stain, and Alamar blue dye were purchased from Bio-Rad (Hercules, CA). Sulfo-SMCC was purchased from Sigma-Aldrich (St Louis, MO). 10 kDa dialysis tubing and DMSO were purchased from Thermo Fisher Scientific (Waltham, MA). Mertansine (DM1) and Live-Dead stain were purchased from Abcam (Cambridge, UK). L1210, P388, EMT6, 4T1, and MCF7 cell lines were purchased from ATCC (Manassas, VA). FBS was purchased from Atlanta Biologicals (Lawrenceville, GA) Penicillin/streptomycin was purchased from Invitrogen (Grand Island, NY).

Methods

Synthesis of the Conjugate

Protein production

Recombinant annexin V was produced was previously described [53]. In brief, E. coli harboring the plasmid containing pET-30 Ek/LIC/ANXA5 were incubated overnight in 100 mL of LB medium with kanamycin. The culture was added to 1 L of fresh LB medium and incubated until the OD of the solution was at 0.5. Protein expression was then induced by adding isopropyl-D-thiogalactopyranoside (IPTG) to the medium and the culture was left to incubate a further 6 hours. The AV expressing bacteria were centrifuged, collected, and sonicated to lyse the cells. The lysate containing all the cellular proteins including the AV protein with an N-terminal six histidine tail was centrifuged and the debris-free supernatant was collected. The supernatant was put through a nickel HisTrap column and was eluted with a 500 mM imidazole buffer. After dialysis the His-tagged protein was cleaved with the HRV 3C protease and purified again on the HisTrap column and dialyzed against a 20 mM sodium phosphate buffer a final time before being flash frozen in liquid nitrogen. The purified protein was quantified using the Bradford assay and analyzed with SDS-PAGE.

Drug Conjugation

Dissolve 1.2 milligrams of sulfo-SMCC in 200 uL of DI water; this is a 100x molar ratio to 1 mg/mL AV, and about a 10x molar ratio for the available lysine residues on AV. All of the sulfo-SMCC solution is added to 1 mg of AV and allowed to react at 4º C for 1 hour. The reacted solution was then dialyzed overnight at 4 ºC with a membrane molecular weight cutoff (MWCO) of 10 kDa against phosphate buffered saline (PBS), pH 7.4.

DM1 (1.0 mg) was dissolved in 150 uL of DMSO; this is a 50x molar ratio to 1 mg/mL annexin, the degree of sulfo-SMCC conjugation determines the number of available maleimide reaction sites. All of the DM1 solution was added to the prepared and dialyzed AV-SMCC conjugate and allowed to react at 4 ºC for 2 hours. The reacted conjugate was dialyzed overnight at 4 ºC with a membrane MWCO of 10 kDa against PBS, pH 7.4.

A Bradford assay was used to determine the final protein concentration. And the extent of DM1 conjugation was determined by reading absorbance at 288 nm of the conjugate and a blank of unconjugated AV at the same protein concentration and comparing to a standard curve. Figure 5 shows the major steps in the reaction.

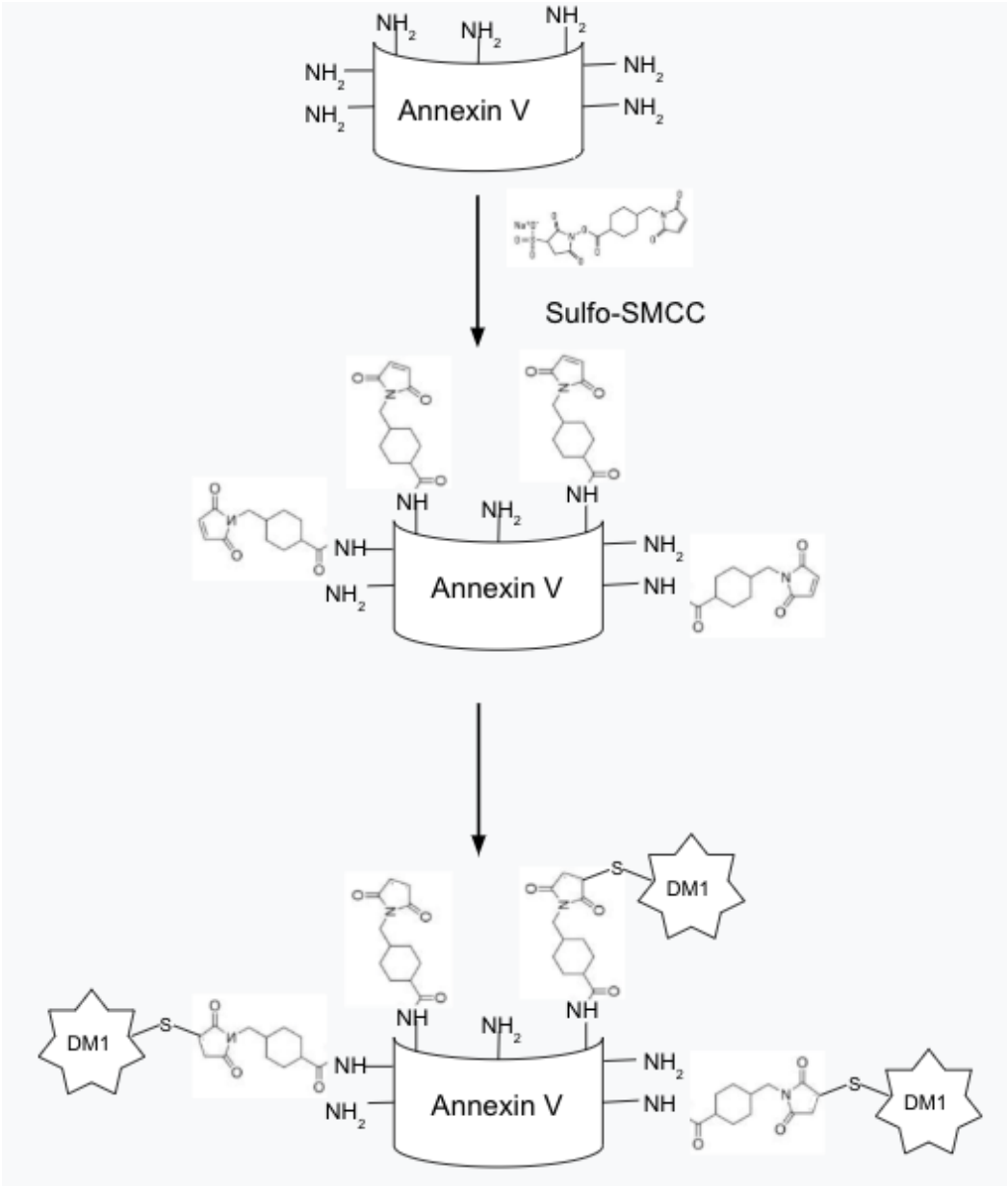

Figure 5. Diagram showing synthesis steps of AV-SMCC-DM1 conjugate.

Characterization

The conjugate was characterized in several ways: SDS-PAGE, absorbance spectroscopy, and mass spectroscopy.

SDS-PAGE

In order to confirm protein modification and estimate the drug loading of the AV protein, 4-20% 10-well gradient gels were purchased and used with 2x Laemmli sample buffer and tris-glycine-SDS running buffer (TGS). The protein and conjugate were each first denatured by the addition of 2.5% 2-mercaptoethanol and heating at 100 ºC for 5 minutes. The samples were run at 200 volts for 25 minutes then stained with Imperial stain and washed in DI water.

Absorbance Spectroscopy

To determine the average number of DM1 molecules per AV protein, the absorbance of the a sample of the conjugate and a sample of the same concentration of unconjugated annexin were measured at 288 nm (DM1 peak absorbance). The peaks were subtracted from each other, to find the contribution of only DM1 to the absorbance at 288 nm. The resulting absorbance value was compared to a standard curve of DM1 concentrations in solution to determine the concentration of DM1 on the proteins. The molar concentration of DM1 was

divided by the molar concentration of the AV protein to arrive at the average DM1 per AV loading.

Mass Spectroscopy

Mass spectroscopy was attempted on the conjugate to get high-resolution data on the distribution of the drug-protein ratios, however the conjugate was too hydrophobic to be used in the mass spectroscopy formulated buffer. As a result, the conjugate precipitated out of solution, and no meaningful data could be collected by mass spectroscopy.

In vitro cytotoxicity

Leukemia

To analyze the in vitro toxicity of the AV-DM1 conjugate compared to unconjugated DM1 in leukemia, two murine leukemia cell lines were used: L1210 and P388. The cells were removed from cryopreservation and cultured in DMEM medium supplemented with 10% FBS and 1% penicillin/streptomycin (Pen/Strep) incubated at 37 ºC and 5% CO_2 until one million cells of each strain were ready to be seeded into two 48-well plates, one for each strain. The cells were seeded at a density of 20,000 cells per 500 uL of DMEM medium per well and incubated for 24 hours to allow the cells to return to a proliferative state. The wells were treated

in quadruplicate groups with 6 concentrations of both the AV-DM1 conjugate and unconjugated DM1. The AV-DM1 treatment concentrations were from 1 pM to 0.1 uM, and the unconjugated DM1 treatment concentrations were from 1 nM to 10 uM. A control plate with untreated cell controls and no-cell blanks was also prepared. The control and treated plates were incubated for 72-hours at 37ºC and 5% CO_2.

After incubation, 20 uL of alamar blue was added to every plate to a final concentration of 10% in each well. The plates were incubated with alamar blue for 2 hours at 37ºC and 5% CO_2 and analyzed in a plate reader using fluorescence with 530 nm excitation and 590 nm emission. The viability was determined by subtracting the no-cell blank from the untreated cell control and treated experimental plates then dividing the average fluorescence of the treated experimental groups by the average of the untreated cell control.

$$\text{Viability\%} = \frac{Treated\ Fluor - Blank}{Untreated\ Fluor - Blank} * 100\%$$

Breast Cancer

To analyze the in vitro toxicity of the AV-DM1 conjugate compared to unconjugated DM1 in breast cancer, three cell lines were used: EMT6 and 4T1 murine breast cancers and MCF7 human breast cancer. Culture medium used for each cell line was different. The medium for EMT6 was Waymouth's medium with 15% FBS, 1% Pen/Strep, for 4T1 was RPMI-1640 with 10% FBS, 1% Pen/Strep; for MCF7 it was EMEM 10% FBS, 1% Pen/Strep. The cells were removed from cryopreservation and cultured in the appropriate medium and incubated at 37 ºC and 5% CO_2 until one million cells of each strain were ready to be seeded into two 96-well plates, one for each strain.

The cells were seeded at a density of 12,000 cells per 200 uL of culture medium per well and incubated for 24 hours to allow the cells to return to a proliferative state. The medium was aspirated and replaced with treated media in sextuplicate groups with eight concentrations of both the AV-DM1 conjugate and unconjugated DM1. The AV-DM1 treatment concentrations were from 0.1 pM to 1 uM, and the unconjugated DM1 treatment concentrations were from 10 pM to 100 uM. A control plate with untreated cell controls and no-cell blanks was also prepared. The control and treated plates were incubated for 72 hours at 37ºC and 5% CO_2.

After incubation, the treatment media was aspirated and fresh media with 20 uL of alamar blue was added to every plate to a final concentration of 10% in each well. The plates were incubated with alamar blue for 2 hours at 37ºC and 5% CO_2 and analyzed in a plate reader using fluorescence with 530 nm excitation and 590 nm emission. The viability was determined by subtracting the no-cell blank from the untreated cell control and treated experimental plates then dividing the average fluorescence of the treated experimental groups by the average of the untreated cell control.

Imaging

Live-Dead Stain and Brightfield Images

A fluorescent live-dead stain was used to image P388 cells grown in DMEM media supplemented with 10% FBS and 1% Pen/Strep to about one million total cells. The cell suspension was split, half in one tube and half in another and centrifuged at 1100 RCF for 5 minutes, and the supernatant was removed from each tube. The cell pellet in one tube was resuspended in normal DMEM media; the pellet in the other tube was resuspended in DMEM media with 2 mM EDTA in order to chelate the calcium ions and prevent the calcium dependent binding of AV to PS. The resuspended cells were plated at 200,000 cells per well in a 24-well plate, and treatment with 1 nM AV-DM1 conjugate began immediately. The treated cells were incubated at 37º C and 5% CO_2 for 3 hours. Brightfield

microscope pictures of the cells were taken at 10x magnification and cells were then stained with the Live-Dead stain for 10 minutes and fluorescence microscope pictures were taken at 10x magnification. Image composites were made in ImageJ.

Chapter III: Results and Discussion

Results

AV-DM1 Conjugation

The conjugation protocol described has been performed several times with average yields of about 1 mg of AV-DM1 conjugate with an average drug-protein ratio of about 8. The DM1 standard curve was made by serial dilutions of DM1 in DMSO with a DMSO blank. At high concentrations (< 1 mM), the peak absorbance of DM1 is shifted higher to 294 nm and gradually shifts lower to around 288 nm as the concentration becomes less as shown in Figure 6.

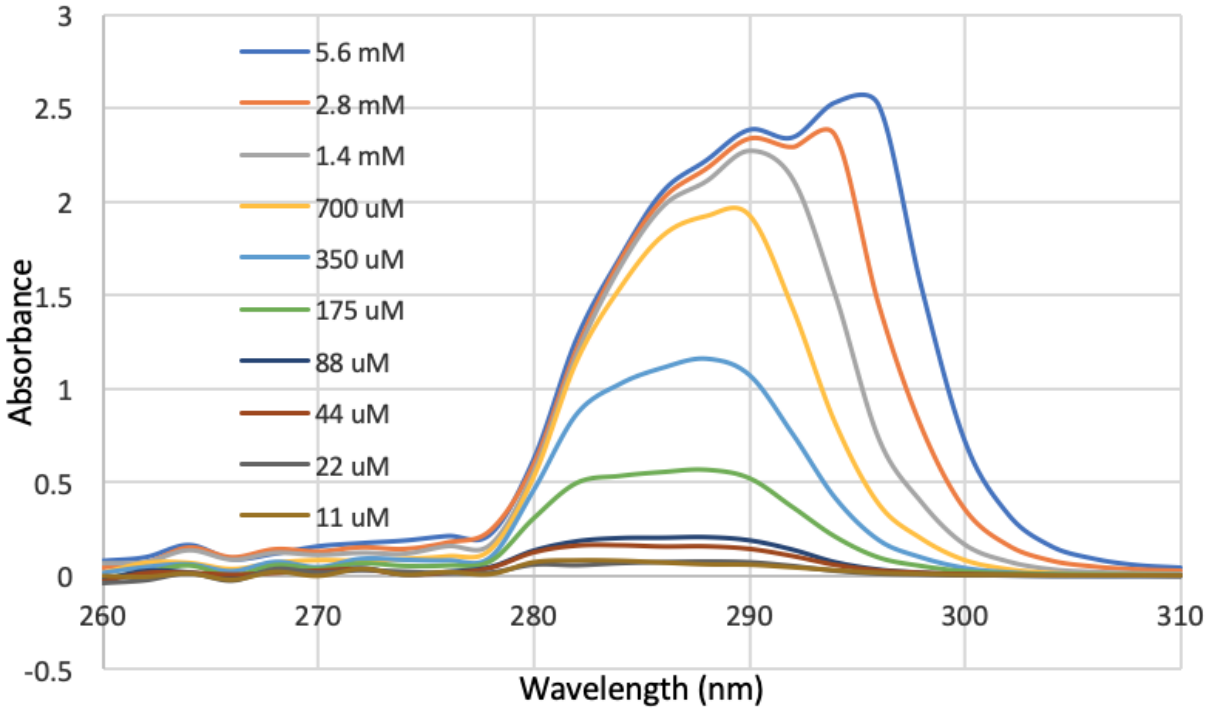

Figure 6. DM1 absorption spectra from 260-310 nm over a range of concentrations from 11 uM to 5.6 mM. The peak absorbance shifts from 294 nm at the highest concentration to 288 nm at the lower concentrations

The standard curve for DM1 in DMSO was determined by taking the absorption values at 288 nm from the above data only until 0.7 mM. Values past 0.7 mM ceased to have a linear relationship between concentration and absorbance as shown in Figure 7.

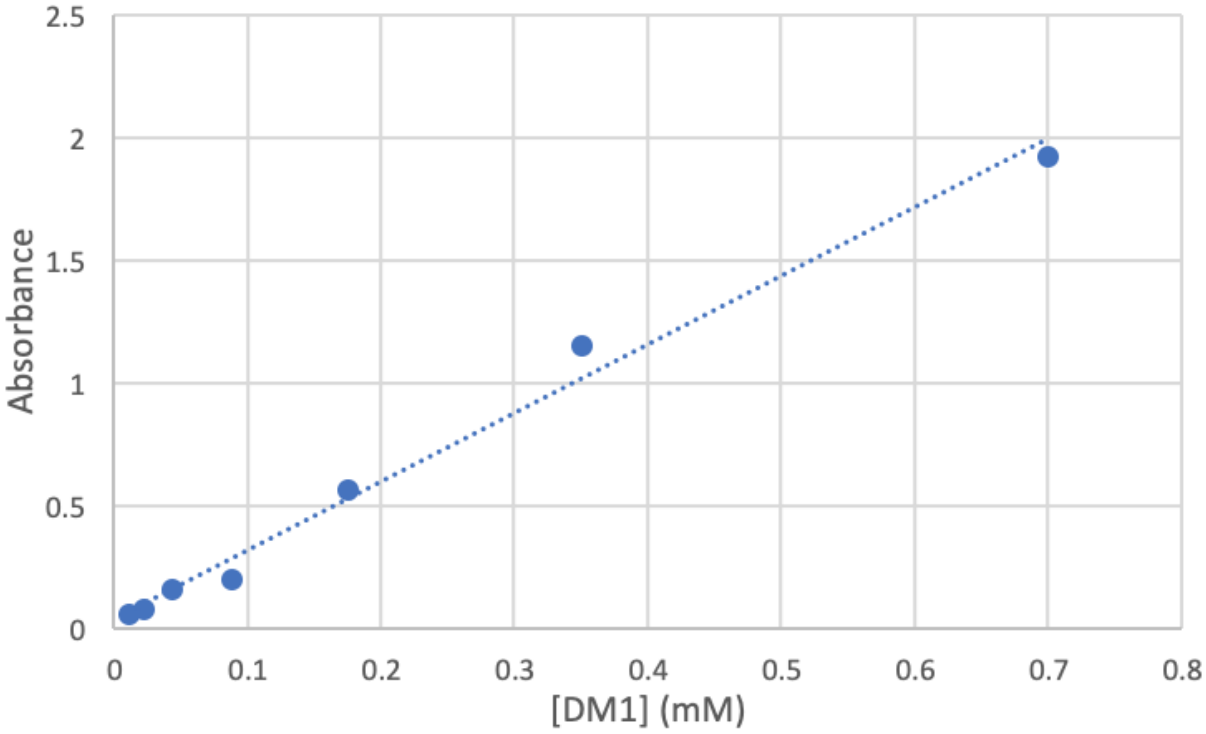

Figure 7. DM1 in DMSO standard curve from 11 uM to 700 uM.

Equation 1. $$Abs = 2.7907 * [DM1] + 0.0406$$

The r^2 value is 0.98899.

The difference in peak absorbances between AV and DM1 is crucial to being able to separate their combined absorbances for analysis of the conjugate. The spectra of both 1 mg/mL AV and 0.15 mM DM1 were taken separately from 200-400 nm. As seen in Figure 8, the gap between peaks is approximately 10 nm.

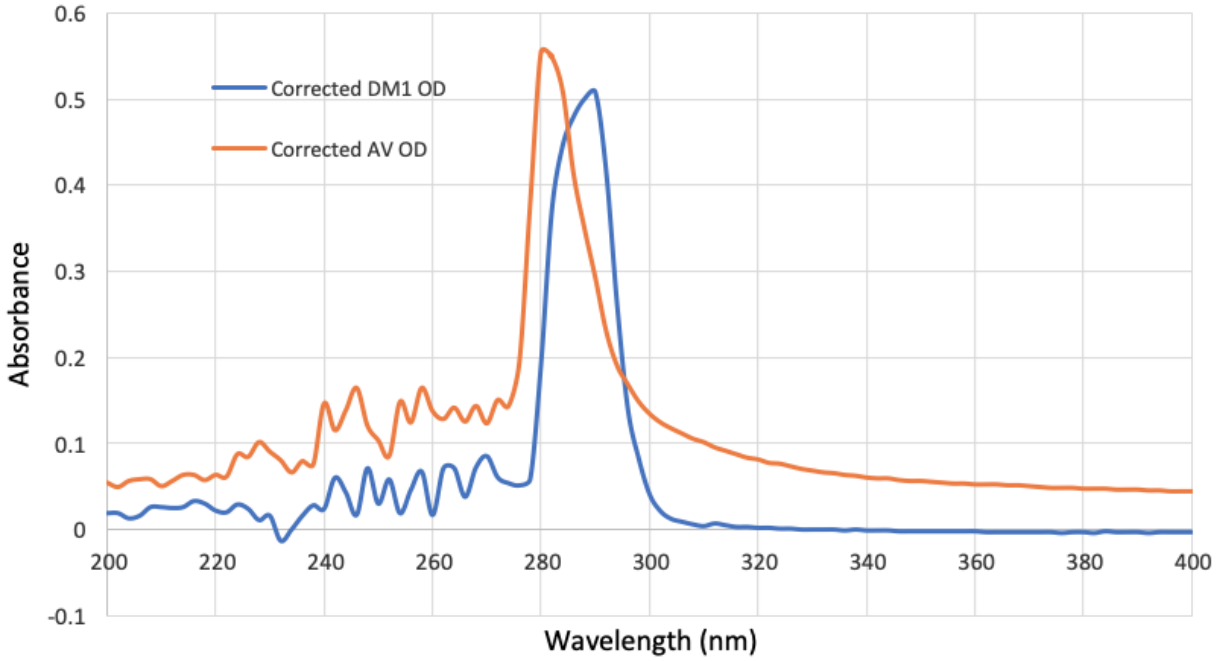

Figure 8. AV and DM1 spectra from 200-400 nm. Samples of pure solvent were subtracted from the individual samples to produce blank-corrected spectra. Peak absorption for 1 mg/mL AV occurred around 280 nm, and 0.15 mM DM1 peak absorption occurred at approximately 290 nm.

The AV-DM1 conjugate was analyzed to determine the degree of drug loading. The absorbance at 288 nm of AV protein at approximately the same concentration of protein as the AV-DM1 conjugate was subtracted from the absorbance of AV-DM1. The resulting value represents the contribution to the absorption of only the DM1 molecules. In the presented data in Figure 9, the peak absorbance contribution from the DM1 was 0.702 at 288 nm. Using the above standard curve equation, that correlates to approximately 0.24 mM DM1. The conjugate at 0.96

mg/mL is a concentration of 0.027 mM. So in this conjugation, the average drug-protein ratio was 8.9 DM1 molecules per AV protein.

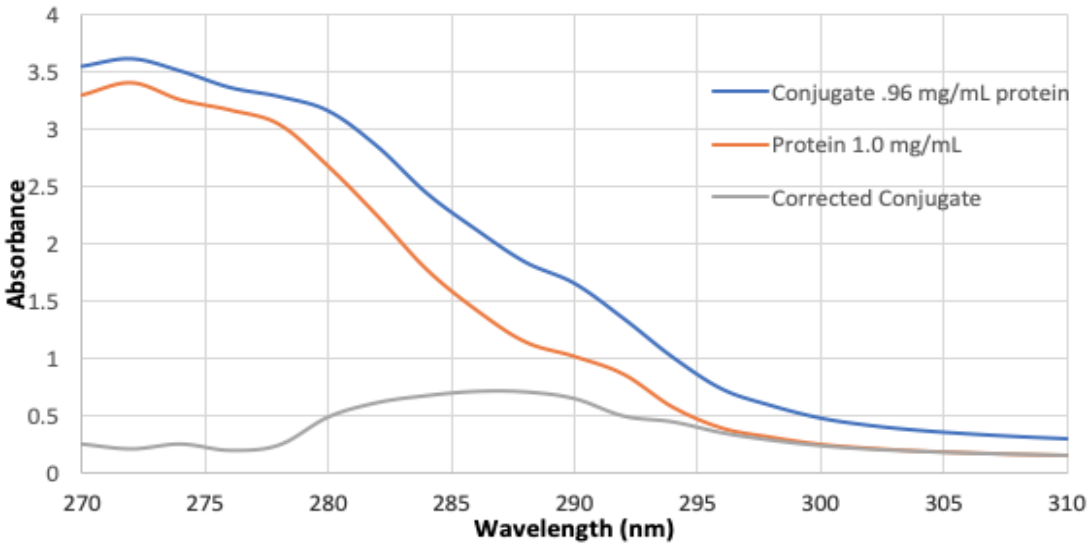

Figure 9. AV-DM1 conjugate and unconjugated AV protein at approximately the same concentration

The AV-DM1 conjugate was analyzed by SDS-PAGE on a 4-20% gradient denaturing gel. SDS-PAGE separates proteins based on size. An electric potential is applied to the gel causing proteins to migrate through the gel. Larger proteins, or proteins with additional modifications in this case, are impeded more relative to smaller, or unconjugated, proteins. As seen in Figure 10, the AV protein in the left-most lane migrated farther than the AV-DM1 conjugate. Also of note is the absence of any bands at multiples of 36 kDa (72, 108 kDa). This is confirmation that no AV-AV polymer products were made in the synthesis.

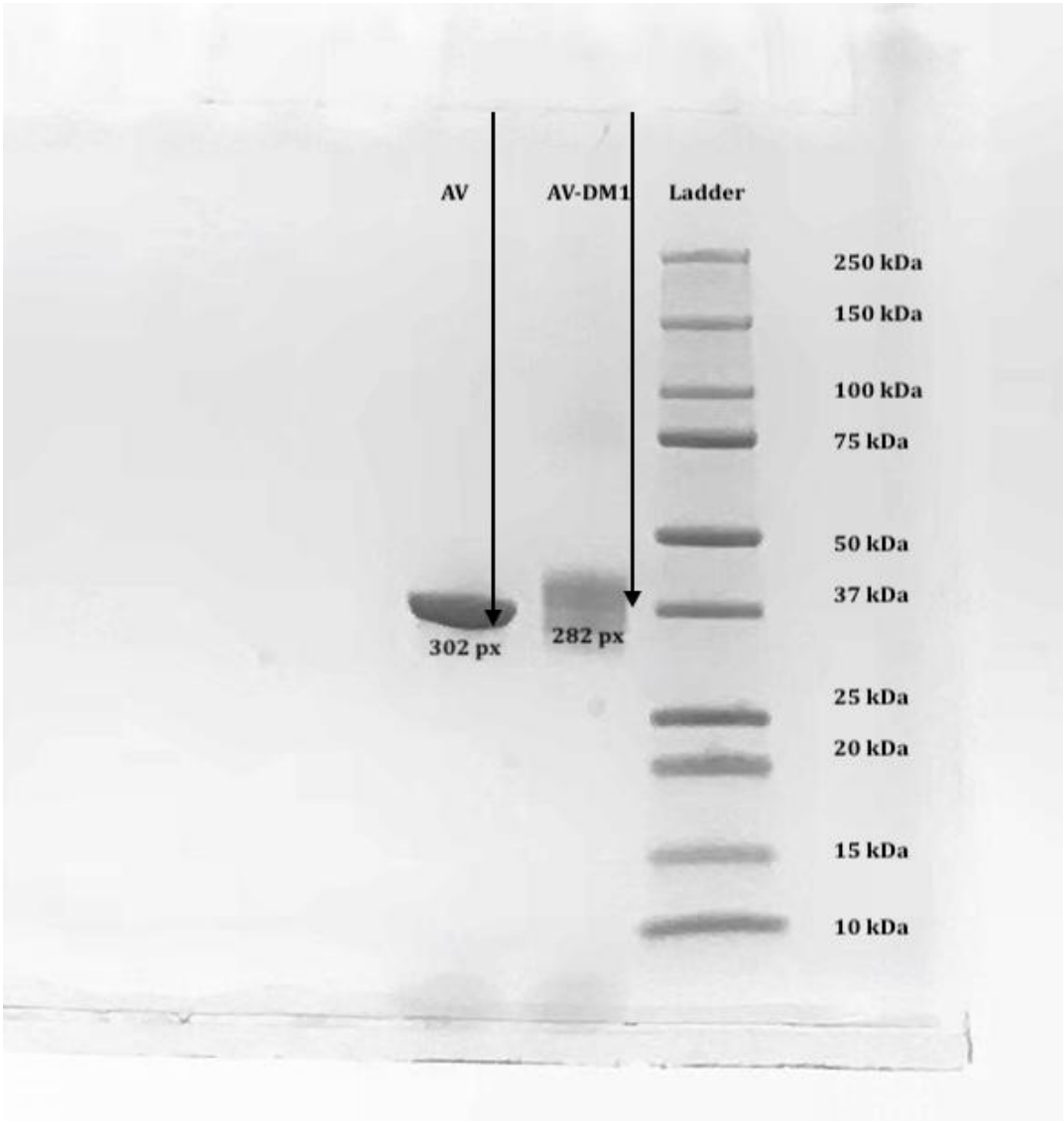

Figure 10. Picture of the SDS-PAGE gel. 5 uL of each the AV protein (1 mg/mL) and AV-DM1 conjugate (0.96 mg/mL) was denatured by boiling with 5 uL Laemmli sample buffer and 0.25 uL of 2-mercaptoethanol. Band migration was measured from bottom of the well to bottom of the band. The AV-DM1 conjugate band was measured to the bottom of the main upper band.

Size can also be estimated from an SDS-PAGE gel. Protein kDa ladder standard migration distances are compared to the dye migration front and paired to the

logarithm of the protein size and plotted as seen in Figure 11. The migration front of the proteins/conjugates with unknown size can be measured and the size can be estimated with the plot made from the protein ladder standards. Once the AV-DM1 conjugate and unconjugated AV sizes were estimated, the difference between them was divided by the combined weight of the linker and drug (about 1 kDa) giving another estimate of the molecules of DM1 per protein. The error associated with SDS-PAGE molecular weight determination is usually within 5-10%. A 5% error associated with the molecular weight of the conjugate is a difference of about 2 kDa, therefore, this method estimates the drug-protein ratio to be 6 ± 2 drug molecules per protein, within the range estimated by the absorption method described.

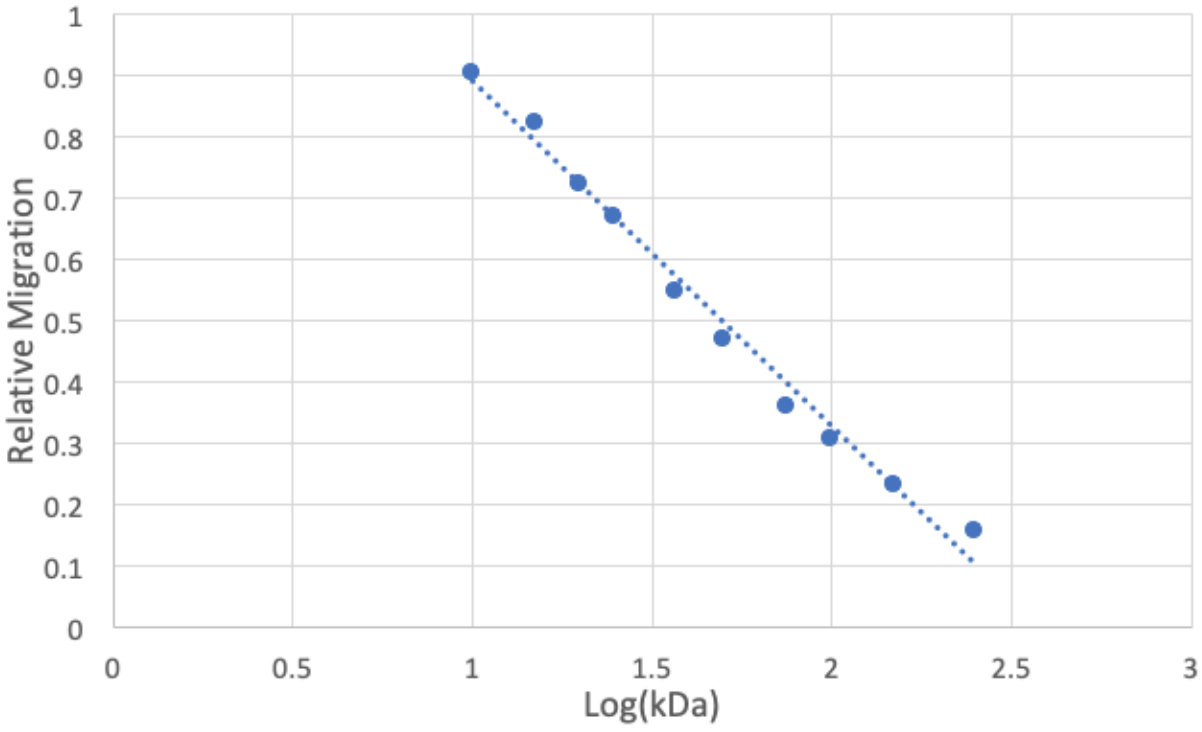

Figure 11. Plot of relative migration of protein standard ladder bands versus the logarithm of their size in kDa. This plot is used to estimate the size of unknown proteins run on the same gel.

Equation 2. $$RM = -0.5623 * log(kDa) + 1.4508$$

The r^2 value is 0.98795.

In Vitro Cytotoxicity

In order to test the toxicity of the AV-DM1 conjugate, several cell lines were treated with many concentrations of the conjugate and compared to treatment with unconjugated DM1. The microtubule inhibiting mechanism of action of DM1 kills cells by mitotic arrest. All five of the cell lines have documented doubling times of 22 or more hours. The standard 24-hour assay would not demonstrate the cytotoxic potential of the drug or conjugate simply because not all cells would have undergone a full cell cycle yet. To demonstrate this, EMT6 cells were used under similar conditions to the 72-hour cytotoxicity assays but treatment was halted after 24 hours and only six of the higher drug concentrations were tested. The results are shown in Figure 12. Neither the drug nor the conjugate showed significant toxicity to EMT6 cells over the 24-hour treatment time.

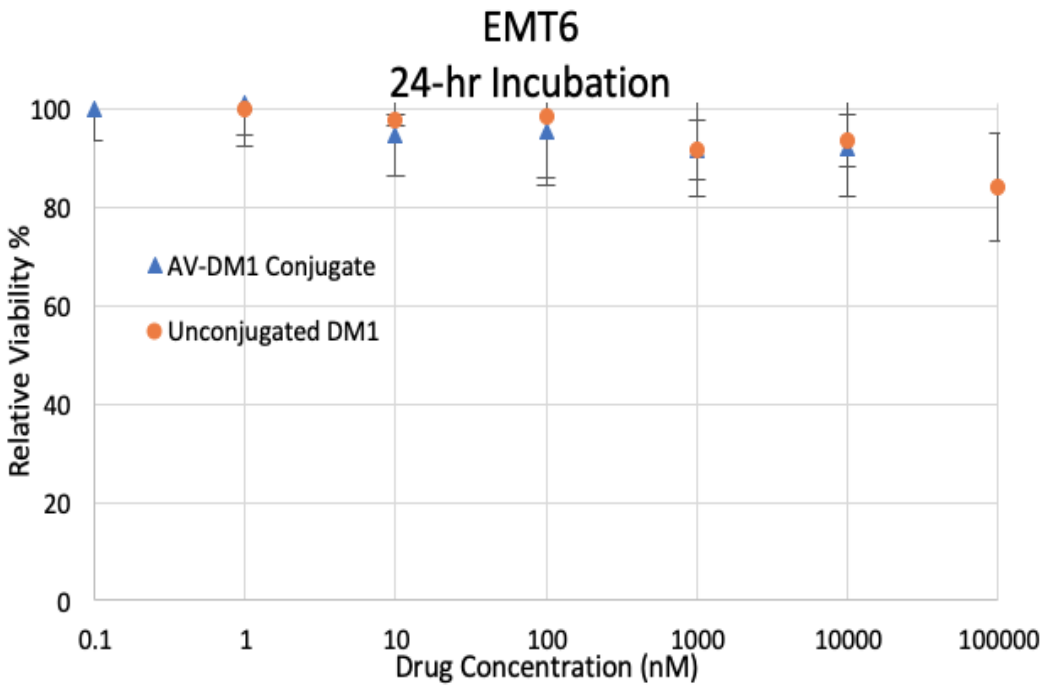

Figure 12. The 24-hour EMT6 cytotoxicity test. Neither of the treatments showed significant toxicity. Data is presented as mean ± SE (n = 6) Untreated cells determined 100% viability.

The 72-hour assays proved to be much more effective against all five cell types. The effectiveness of the treatments was assessed by their EC50, the concentration of a drug were 50% effectiveness is reached in a given time period. The lower the EC50, the less of a drug is needed to achieve the half-maximal response. The EC50 is derived from the dose response curves by using the sum of squared differences to fit a sigmoidal regression of the form:

Equation 3. $$V = \frac{Max}{1+(\frac{C}{EC50})^H}$$

Where V is the response (viability in this context), Max is the theoretical maximum response (100% viability), C is the concentration of drug, EC50 is the concentration of half-maximal effectiveness, and H is the Hill coefficient which describes how "steep" the curve is.

The results for the breast cancer tumors are below: EMT6 in Figure 13, 4T1 in Figure 14, and MCF7 in Figure 15. Results for the P388 leukemia is in Figure 16 and for the L1210 leukemia is in Figure 17.

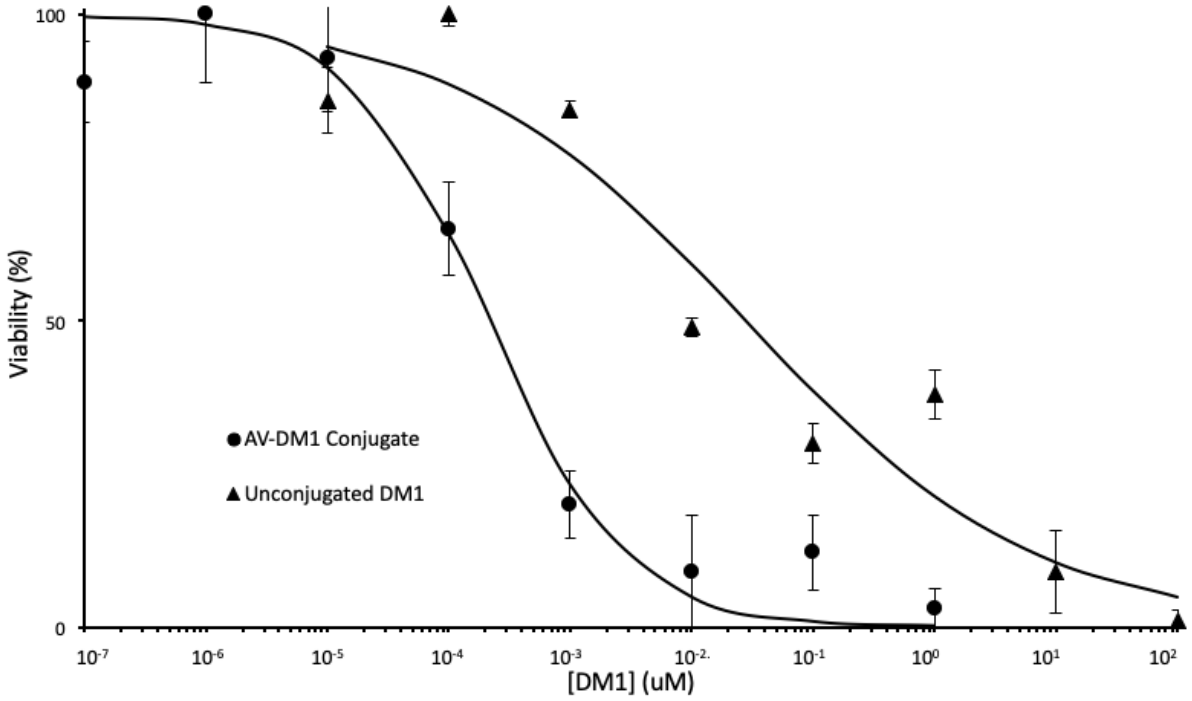

Figure 13. Results for EMT6 murine breast cancer cell line cytotoxicity of the AV-DM1 conjugate and unconjugated DM1. The EC50 is 0.21 nM for the AV-DM1 conjugate and 28 nM for unconjugated DM1. This is an increase in effectivity of 130x. Data is presented as mean ± SE (n = 6).

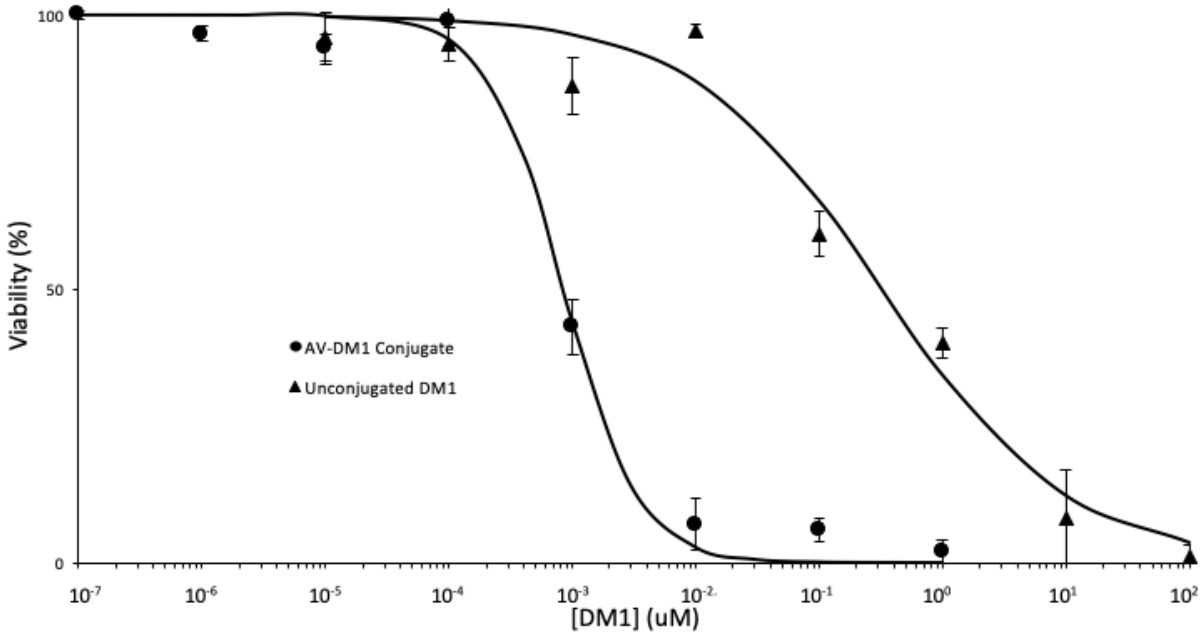

Figure 14. Results for 4T1 murine breast cancer cell line cytotoxicity of the AV-DM1 conjugate and unconjugated DM1. The EC50 is 0.85 nM for the AV-DM1 conjugate and 320 nM for unconjugated DM1. This is an increase in effectivity of 377x. Data is presented as mean ± SE (n = 6).

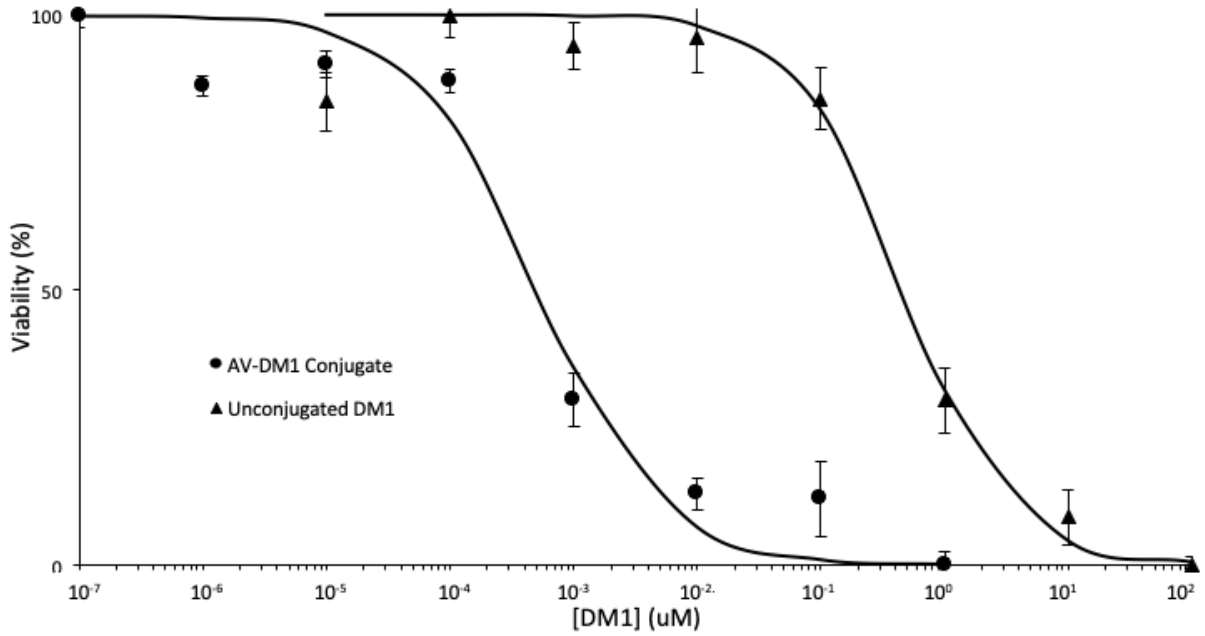

Figure 15. Results for MCF7 human breast cancer cell line cytotoxicity of the AV-DM1 conjugate and unconjugated DM1. The EC50 is 0.52 nM for the AV-DM1 conjugate and 473 nM for unconjugated DM1. This is an increase in effectivity of 910x. Data is presented as mean ± SE (n = 6).

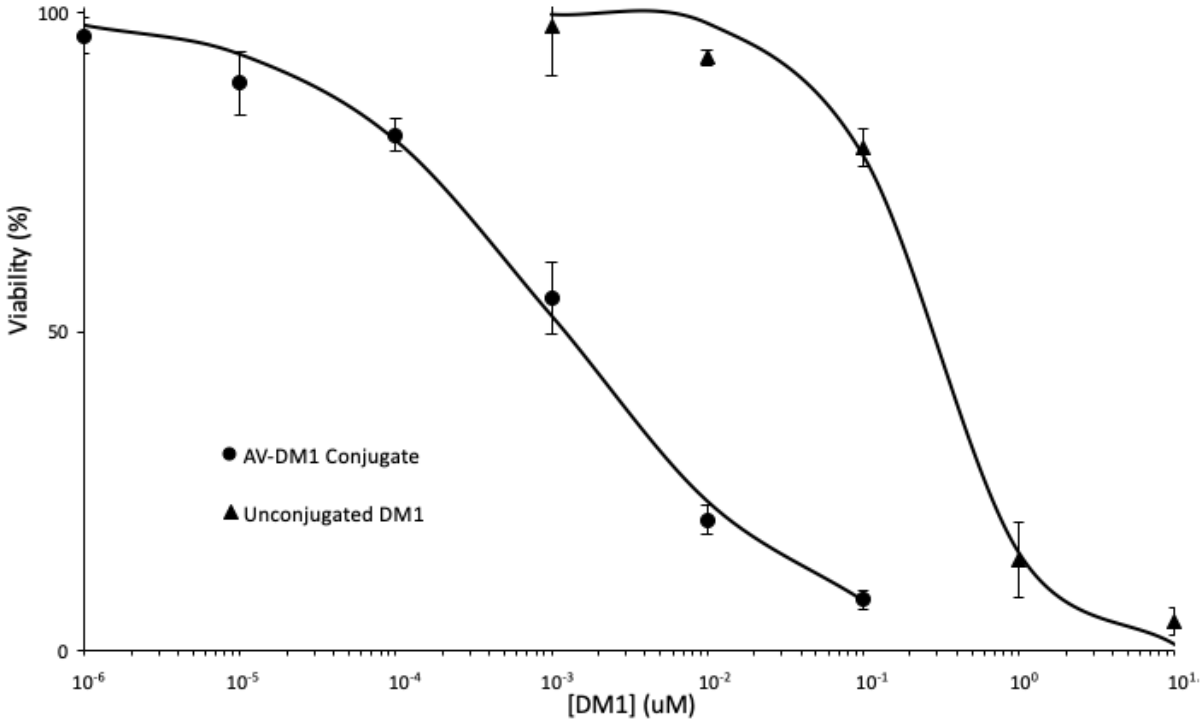

Figure 16. Results for P388 murine leukemia cell line cytotoxicity of the AV-DM1 conjugate and unconjugated DM1. The EC50 is 1.2 nM for the AV-DM1 conjugate and 264 nM for unconjugated DM1. This is an increase in effectivity of 221x. Data is presented as mean ± SE (n = 6).

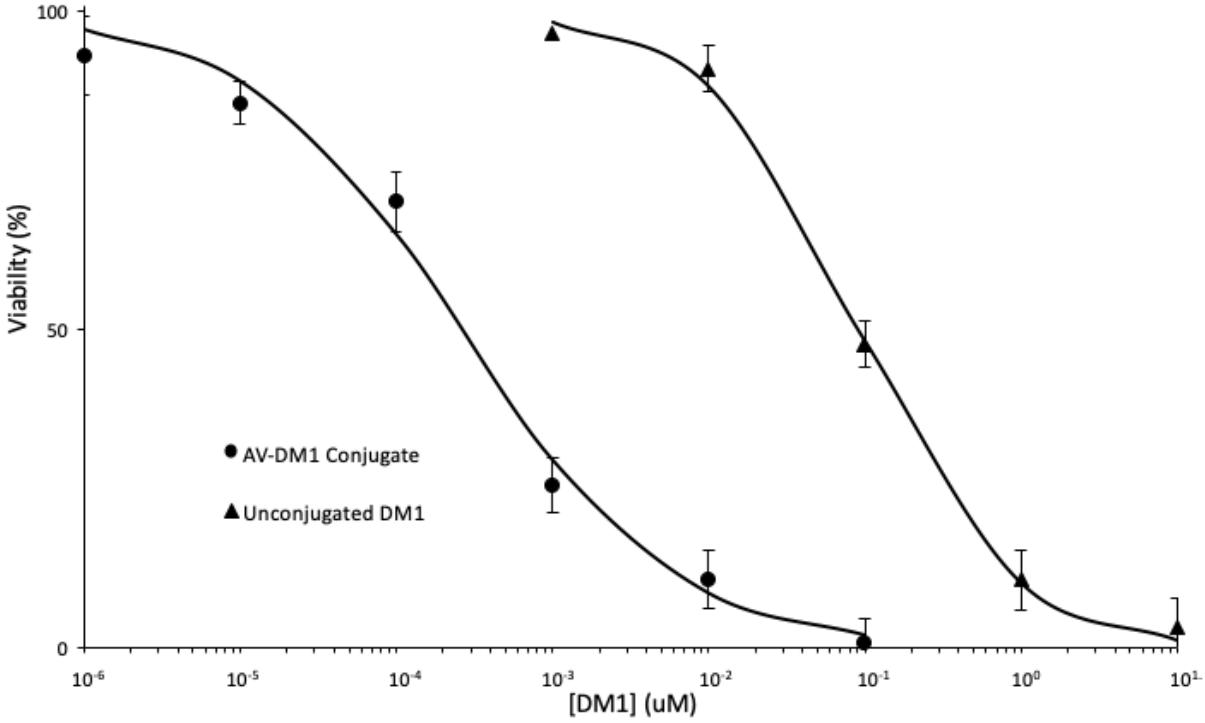

Figure 17. Results for L1210 murine leukemia cell line cytotoxicity of the AV-DM1 conjugate and unconjugated DM1. The EC50 is 0.26 nM for the AV-DM1 conjugate and 93 nM for unconjugated DM1. This is an increase in effectivity of 354x. Data is presented as mean ± SE (n = 6).

Imaging

Brightfield and fluorescence imaging was done on P388 cells in order to qualitatively analyze both the viability and morphology of cells treated with the AV-DM1 conjugate and to demonstrate the binding specificity of the conjugate. A live-dead stain was used to indicate the viability of the cells. A membrane-permeable non-fluorescent dye that is converted to a green fluorescent form in

metabolically active cells stains for viable cells. Propidium iodide is membrane-impermeable red fluorescent dye that binds DNA in cells with damaged membranes. The cells were treated for a period of only 3 hours. This was done in order to maintain the viability of cells in the EDTA-supplemented control group. EDTA chelates calcium ions which prevents efficient binding of the AV-DM1 conjugate, but calcium is also necessary for long term cell viability. Only a small portion of cells in the treatment group would enter metaphase of the mitotic cycle in the 3 hour period, and even fewer would remain arrested there long enough to exhibit signs of apoptosis like membrane damage. Still, notably differences were seen between the EDTA and treatment groups in both brightfield and fluorescent microscope images. Brightfield images are shown in Figure 18 and Figure 19. Fluorescence images are shown in Figure 20 and Figure 21.

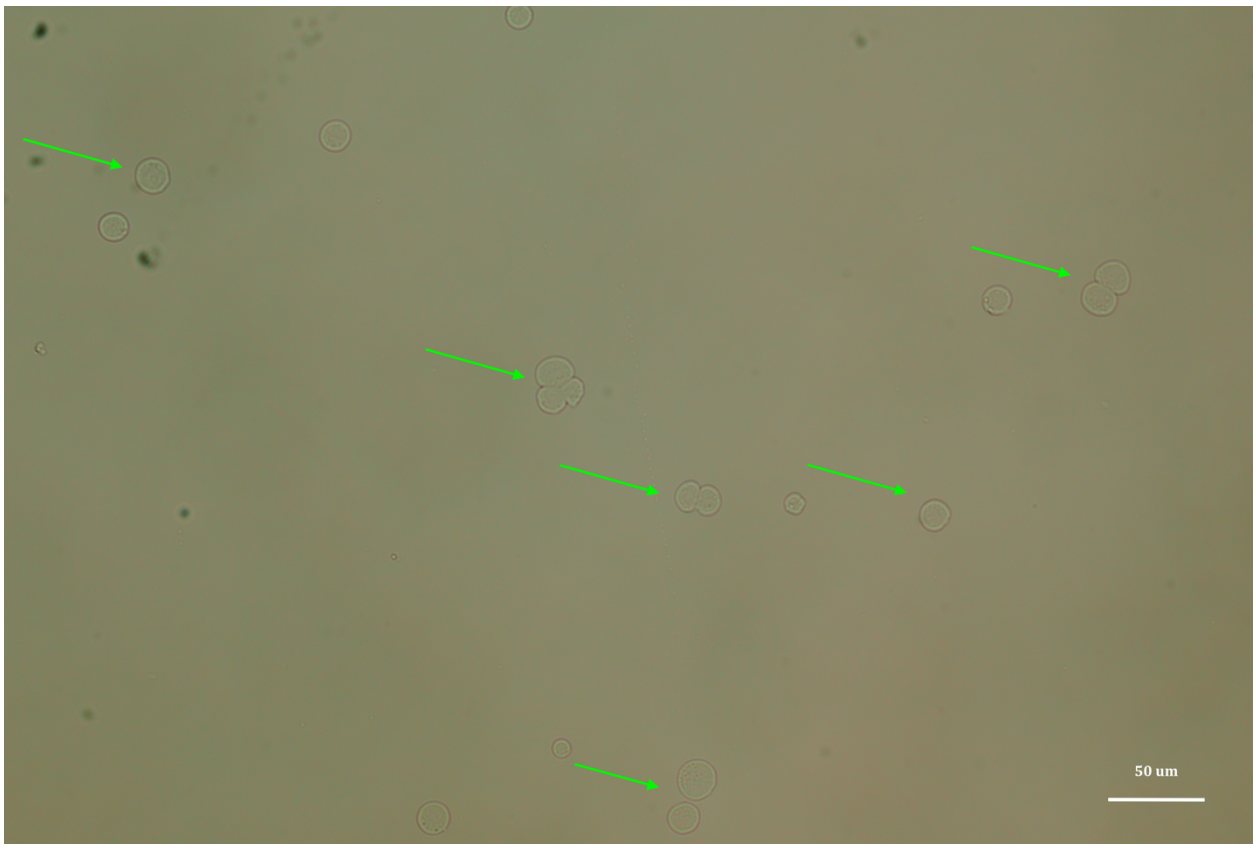

Figure 18. Brightfield microscope image of P388 cells incubated for 3 hours with 2 mM EDTA supplemented DMEM media and treated with calcium dependent AV-DM1 cytotoxic conjugate. Cell division has not been impaired and cells appear to be intact as indicated with green arrows in the figure.

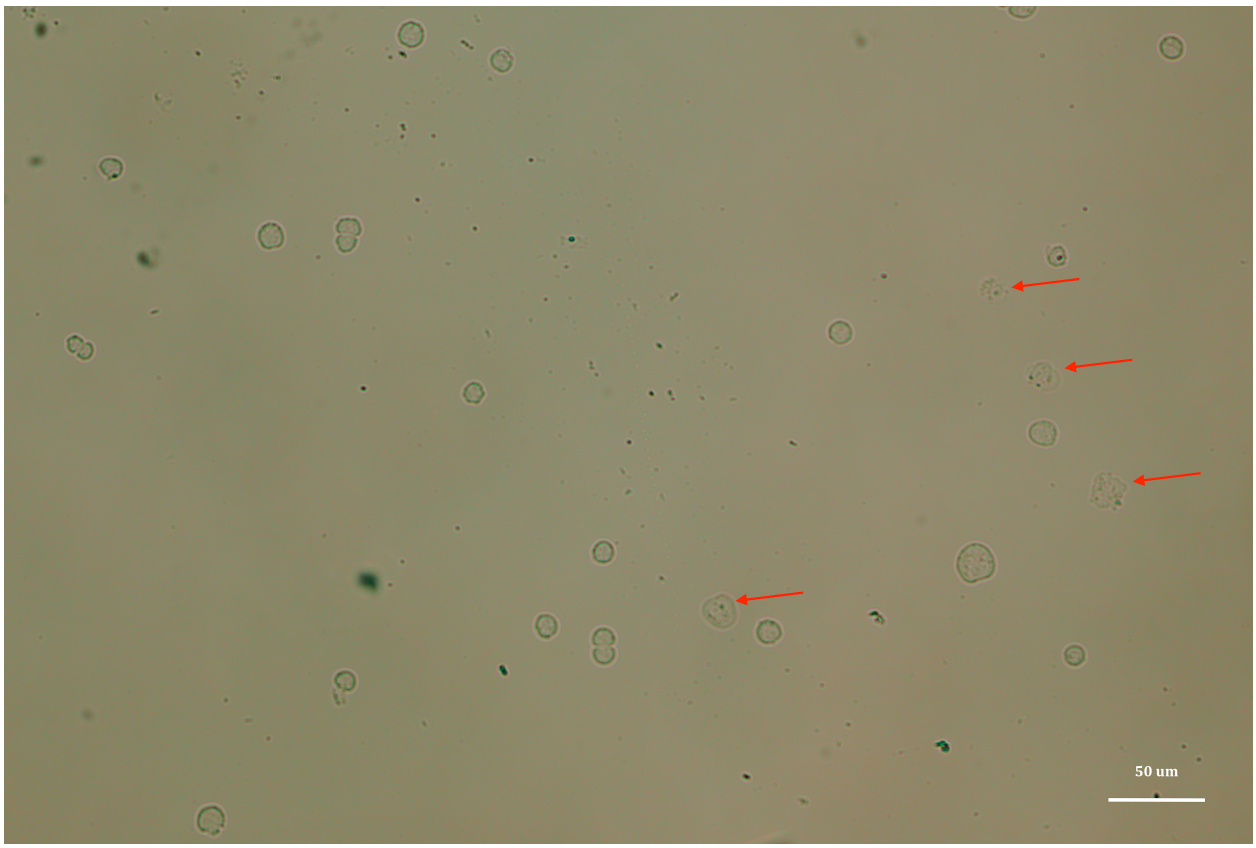

Figure 19. Brightfield microscope image of P388 cells incubated for 3 hours with 1.2 mM calcium DMEM media and treated with calcium dependent AV-DM1 cytotoxic conjugate. Cell division has been slightly hindered, cells appear to not be as large as the EDTA treatment group. Some cells appear to be apoptotic with damaged membranes and have been marked with red arrows.

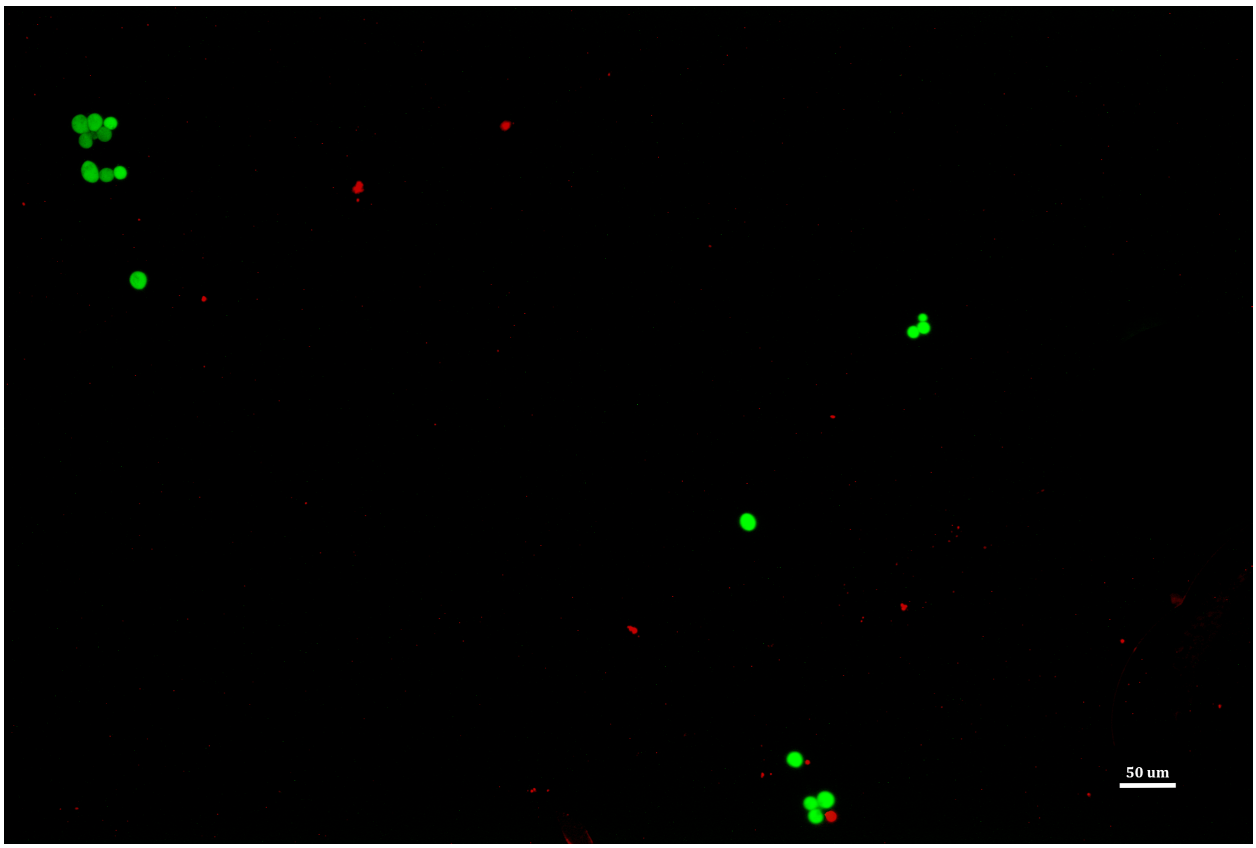

Figure 20. Live-Dead stained fluorescence microscope image of P388 cells incubated for 3 hours with 2 mM EDTA supplemented DMEM media and treated with calcium dependent AV-DM1 cytotoxic conjugate. Cell division has not been impaired and the vast majority of cells appear to be healthy and metabolically active with intact cell membranes. Dead cells appear red due to propidium iodide binding to intracellular DNA.

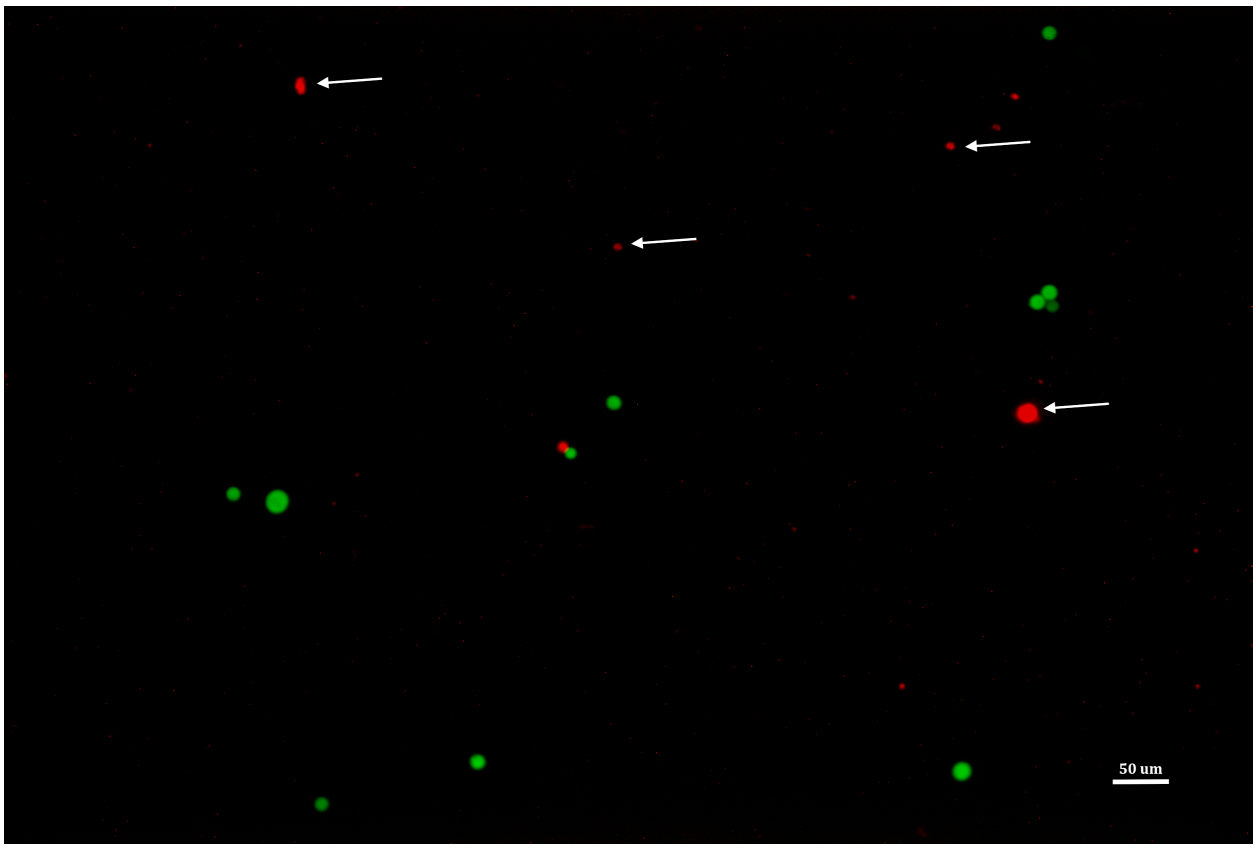

Figure 21. Live-Dead stained fluorescence microscope image of P388 cells incubated for 3 hours with 1.2 mM calcium DMEM media and treated with calcium dependent AV-DM1 cytotoxic conjugate. Cell division has been notably impaired compared to the EDTA treatment group and a greater portion of cells have compromised membranes, shown with white arrows. Dead cells appear red due to propidium iodide binding to intracellular DNA.

Discussion

AV-DM1 Conjugation

The conjugation and subsequent characterization of the AV-DM1 drug has many implications in the literature. The most commonly cited "ideal" drug ratio for antibody conjugates is three to five drugs per antibody. The logic that the more drugs that can be linked to a targeting protein, the more effective only holds up to a certain extent in mouse models. As the number of drug molecules on the protein increases, so does the overall hydrophobicity of the drug conjugate. Conjugates with higher hydrophobicity have shown higher rates of *in vivo* plasma clearance and less time in vascular circulation. Conjugates with eight conjugated hydrophobic drug molecules showed up to three times faster blood clearance than conjugates with four drugs per antibody. However, hydrophobicity is generally associated with more efficient uptake by the lymphatic system, not necessarily higher rates of degradation. More hydrophobic conjugates like antibody-DM1 conjugates can have lymphatic residence half-lives of up to 7 days, though vascular circulation half-lives tend to be around 2-3 days [54-58].

The conjugate that was synthesized had approximately eight drugs per 35 kDa protein. This is compared to Kadcyla (trastuzumab-emtansine) with about four drugs per 148 kDa protein [59]. The AV-DM1 conjugate proved very difficult to analyze with mass spectroscopy at least in part due to its high hydrophobicity. Although it proved effective *in vitro*, that success may be limited in follow-up

mouse tumor model experiments due to the potential for a high rate of clearance from the plasma and a short window to bind to and act on the tumor vasculature. The drug protein ratio may need to be lowered in order to effectively treat *in vivo* tumors.

In Vitro Cytotoxicity

The AV-DM1 conjugate showed remarkable increases in toxicity compared to the unconjugated DM1. The range of EC50s for unconjugated DM1 (~20-400 nM), matches well with literature values for a range of cell lineages. Although early publications on DM1 reported EC50s in the range of 1-10 pM, more recent literature has reported values from 1 nM to 1 uM [60, 61]. The AV-DM1 conjugate also showed comparable activity to antibody-drug conjugates in the literature. AV-DM1 had a range from about 200 pM to 1.2 nM in the breast cancer and leukemia cells tested. Most literature reports in vitro EC50 values of 100 pM to 10 nM [48, 62-63]. Kadcyla (trastuzumab-DM1) commonly has EC50 values of about 3 nM in non-Hodgkins lymphoma [64], huN901-DM1 has EC50 values between 60 pM and 300 pM for various tumor lineages including colorectal cancer, lung cancers, and neuroblastoma [65].

Chapter IV: Conclusions

Conclusion

Chemotherapy has taken advantage of the narrow difference in toxicities of antineoplastic drugs between healthy cells and tumor cells. With the advent of targeted drugs, that difference can be widened, more potent and effective drugs can be used, and patients will not have to suffer as debilitating side effects. In pursuit of that goal, the AV-DM1 conjugate that has been synthesized, characterized, and tested has shown great potential as a cancer therapeutic. The synthesis is simple and quick with scalable chemistry. It is more potent by over 100x than conventional chemotherapeutics. AV is highly selective in binding and is generalizable to many diverse types of solid tumor vasculatures and leukemias. However there are still many unanswered questions in regards to how well it will perform in vivo. The clearance and immune response to a highly conjugated small protein may be too high, and a lower drug protein ratio may be more useful for mouse models. Nevertheless, the preliminary work on the AV-DM1 conjugate warrants investigation into potential in vivo applications and beyond.

Future Directions

With the clinical success shown by mainstream antibody-drug conjugates and especially by antibody-maytansinoid conjugates, there is every reason to move forward with investigating new approaches to make these treatments more widely available. Annexin V-DM1 has shown remarkable in vitro results comparable in specificity and toxicity to current antibody-drug conjugates in clinical use. Preclinical in vivo work is the next major step for the AV-DM1 conjugate, beginning with dosing studies. Studies involving conjugates using antibodies with a high drug to protein ratio (6-8) tended to show maximum tolerated doses of around 50-100 mg/kg [65]. More normal doses for treatment tend to be around 0.1 - 0.5 mg/kg [64-66]. Eventually the AV-DM1 conjugate should be compared to current standard clinical treatments in leukemia and metastatic breast cancer, chlorambucil and doxorubicin respectively. Also of use may be a direct comparison to trastuzumab-DM1 in a mouse breast cancer xenograft model.

References

1. Hanahan D, Weinberg RA. Hallmarks of cancer: the next generation. *Cell*. 2011;144(5):646-674. doi:10.1016/j.cell.2011.02.013

2. Levine AJ, Puzio-Kuter AM. The Control of the Metabolic Switch in Cancers by Oncogenes and Tumor Suppressor Genes. Science. 2010;330(6009):1340-1344. doi:10.1126/science.1193494

3. Ghebranious N, Donehower LA. Mouse models in tumor suppression. *Oncogene*. 1998;17(25):3385-3400. doi:10.1038/sj.onc.1202573

4. Philippi C, Loretz B, Schaefer UF, Lehr CM. Telomerase as an emerging target to fight cancer--opportunities and challenges for nanomedicine. *J Control Release*. 2010;146(2):228-240. doi:10.1016/j.jconrel.2010.03.025

5. Heerboth S, Housman G, Leary M, Longacre M, Byler S, Lapinska K, Willbanks A, Sarkar S. EMT and tumor metastasis. *Clin Transl Med*. 2015;4. doi:10.1186/s40169-015-0048-3

6. Nguyen DX, Bos PD, Massagué J. Metastasis: from dissemination to organ-specific colonization. *Nat Rev Cancer*. 2009;9(4):274-284. doi:10.1038/nrc2622

7. Ran S, Thorpe PE. Phosphatidylserine is a marker of tumor vasculature and a potential target for cancer imaging and therapy. *Int J Radiat Oncol Biol Phys*. 2002;54(5):1479-1484.

8. Devaux PF. Protein involvement in transmembrane lipid asymmetry. *Annu Rev Biophys Biomol Struct*. 1992;21:417-439. doi:10.1146/annurev.bb.21.060192.002221

9. Comfurius P, Senden JM, Tilly RH, Schroit AJ, Bevers EM, Zwaal RF. Loss of membrane phospholipid asymmetry in platelets and red cells may be associated with calcium-induced shedding of plasma membrane and inhibition of aminophospholipid translocase. *Biochim Biophys Acta*. 1990;1026(2):153-160.

10. Zhou Q, Zhao J, Stout JG, Luhm RA, Wiedmer T, Sims PJ. Molecular cloning of human plasma membrane phospholipid scramblase. A protein mediating transbilayer movement of plasma membrane phospholipids. *J Biol Chem*. 1997;272(29):18240-18244.

11. Utsugi T, Schroit AJ, Connor J, Bucana CD, Fidler IJ. Elevated expression of phosphatidylserine in the outer membrane leaflet of human tumor cells and recognition by activated human blood monocytes. *Cancer Res*. 1991;51(11):3062-3066.

12. Zwaal RFA, Comfurius P, Bevers EM. Surface exposure of phosphatidylserine in pathological cells. *Cell Mol Life Sci*. 2005;62(9):971-988. doi:10.1007/s00018-005-4527-3

13. Riedl S, Rinner B, Asslaber M, Schaider H, Walzer S, Novak A, Lohner K, Zweytick D. In search of a novel target - phosphatidylserine exposed by non-apoptotic tumor cells and metastases of malignancies with poor treatment efficacy. *Biochim Biophys Acta*. 2011;1808(11):2638-2645. doi:10.1016/j.bbamem.2011.07.026

14. Hillen F, Griffioen AW. Tumour vascularization: sprouting angiogenesis and beyond. *Cancer Metastasis Rev*. 2007;26(3-4):489-502. doi:10.1007/s10555-007-9094-7

15. Shi J, Kantoff PW, Wooster R, Farokhzad OC. Cancer nanomedicine: progress, challenges and opportunities. *Nat Rev Cancer*. 2017;17(1):20-37. doi:10.1038/nrc.2016.108

16. Bazak R, Houri M, Achy SE, Hussein W, Refaat T. Passive targeting of nanoparticles to cancer: A comprehensive review of the literature. *Mol Clin Oncol*. 2014;2(6):904-908. doi:10.3892/mco.2014.356

17. Bertrand N, Wu J, Xu X, Kamaly N, Farokhzad OC. Cancer nanotechnology: the impact of passive and active targeting in the era of modern cancer biology. *Adv Drug Deliv Rev*. 2014;66:2-25. doi:10.1016/j.addr.2013.11.009

18. Andree HA, Reutelingsperger CP, Hauptmann R, Hemker HC, Hermens WT, Willems GM. Binding of vascular anticoagulant alpha (VAC alpha) to planar phospholipid bilayers. *J Biol Chem*. 1990;265(9):4923-4928.

19. Schutters K, Reutelingsperger C. Phosphatidylserine targeting for diagnosis and treatment of human diseases. *Apoptosis*. 2010;15(9):1072-1082. doi:10.1007/s10495-010-0503-y

20. van Genderen HO, Kenis H, Hofstra L, Narula J, Reutelingsperger CPM. Extracellular annexin A5: Functions of phosphatidylserine-binding and two-dimensional crystallization. *Biochimica et Biophysica Acta (BBA) - Molecular Cell Research*. 2008;1783(6):953-963. doi:10.1016/j.bbamcr.2008.01.030

21. Huber R, Schneider M, Mayr I, Römisch J, Paques EP. The calcium binding sites in human annexin V by crystal structure analysis at 2.0 A resolution. Implications for membrane binding and calcium channel activity. *FEBS Lett*. 1990;275(1-2):15-21.

22. Kenis H, Genderen H van, Bennaghmouch A, Rinia HA, Frederik P, Narula J, Hofstra L, Reutelingsperger CPM. Cell Surface-expressed Phosphatidylserine and Annexin A5 Open a Novel Portal of Cell Entry. *J Biol Chem*. 2004;279(50):52623-52629. doi:10.1074/jbc.M409009200

23. National Cancer Act of 1971. National Cancer Institute. https://www.cancer.gov/about-nci/legislative/history/national-cancer-act-1971. Published February 16, 2016. Accessed April 22, 2019.

24. Barker AD, Jordan H. Legislative History of the National Cancer Program. *Holland-Frei Cancer Medicine 6th edition*. 2003. https://www.ncbi.nlm.nih.gov/books/NBK13873/. Accessed April 22, 2019.

25. Kupchan SM, Komoda Y, Court WA, Thomas GJ, Smith RM, Karim A, Gilmore CJ, Haltiwanger RC, Bryan RF. Tumor inhibitors. LXXIII. Maytansine, a novel antileukemic ansa macrolide from Maytenus ovatus. Journal of the American Chemical Society. 1972;94(4):1354-1356. doi:10.1021/ja00759a054

26. Douros J, Suffness M. The National Cancer Institute's Natural Products Antineoplastic Development Program. In: Carter SK, Sakurai Y, eds. *New Anticancer Drugs*. Recent Results in Cancer Research. Berlin, Heidelberg: Springer Berlin Heidelberg; 1980:21-44. doi:10.1007/978-3-642-81392-4_3

27. Kupchan SM, Komoda Y, Branfman AR, Dailey RG, Zimmerly VA. Tumor inhibitors. 96. Novel maytansinoids. Structural interrelations and requirements for antileukemic activity. Journal of the American Chemical Society. 1974;96(11):3706-3708. doi:10.1021/ja00818a086

28. Wolpert-DeFilippes MK, Bono VH, Dion RL, Johns DG. Initial studies on maytansine-induced metaphase arrest in 11210 mürine leukemia cells. *Biochemical Pharmacology*. 1975;24(18):1735-1738. doi:10.1016/0006-2952(75)90017-9

29. Wolpert-Defilippes MK, Adamson RH, Cysyk RL, Johns DG. Initial studies on the cytotoxic action of maytansine, a novel ansa macrolide. *Biochemical Pharmacology*. 1975;24(6):751-754. doi:10.1016/0006-2952(75)90257-9

30. Bhattacharyya B, Wolff J. Maytansine binding to the vinblastine sites of tubulin. *FEBS Letters*. 1977;75(1-2):159-162. doi:10.1016/0014-5793(77)80075-6

31. Issell BF, Crooke ST. Maytansine. *Cancer Treatment Reviews*. 1978;5(4):199-207. doi:10.1016/S0305-7372(78)80014-0

32. Cabanillas F, Bodey GP, Burgess MA, Freireich EJ. Results of a phase II study of maytansine in patients with breast carcinoma and melanoma. *Cancer Treat Rep*. 1979;63(3):507-509.

33. Rosenthal S, Harris DT, Horton J, Glick JH. Phase II study of maytansine in patients with advanced lymphomas: an Eastern Cooperative Oncology Group pilot study. *Cancer Treat Rep*. 1980;64(10-11):1115-1117.

34. Franklin R, Samson M, Fraile R, Abu-Zahra H, O'Bryan R, Baker L. A Phase I-II Study of Maytansine Utilizing a Weekly Schedule. Cancer. 1980;46:1104-1108.

35. Goldmacher VS, Blättler WA, Lambert JM, Chari RVJ. Immunotoxins and Antibody-Drug Conjugates for Cancer Treatment. In: Muzykantov V, Torchilin

V, eds. *Biomedical Aspects of Drug Targeting*. Boston, MA: Springer US; 2002:291-309. doi:10.1007/978-1-4757-4627-3_15

36. Chari RVJ, Martell BA, Gross L, Cook B, Shah SA, Blather WA, McKenzie SJ, Goldmacher' VS. Immunoconjugates Containing Novel Maytansinoids: Promising Anticancer Drugs. :6.

37. Chari RJ, Goldmacher VS, Lambert JM, Blattler WA. Cytotoxic agents comprising maytansinoids and their therapeutic use. May 1993. https://patents.google.com/patent/US5208020A/en. Accessed April 22, 2019.

38. Goldmacher VS, Blättler WA, Lambert JM, Chari RVJ. Immunotoxins and Antibody-Drug Conjugates for Cancer Treatment. In: Muzykantov V, Torchilin V, eds. *Biomedical Aspects of Drug Targeting*. Boston, MA: Springer US; 2002:291-309. doi:10.1007/978-1-4757-4627-3_15

39. Lambert JM, Chari RVJ. Ado-trastuzumab Emtansine (T-DM1): An Antibody–Drug Conjugate (ADC) for HER2-Positive Breast Cancer. J Med Chem. 2014;57(16):6949-6964. doi:10.1021/jm500766w

40. Geller JI, Pressey JG, Smith MA, Kudgus RA, Schoon R, McGovern RM, Cajaiba M, Reid JM, Hall D, Barkauskas DA, Dome J, Fox E, Weigel B. ADVL1522: A phase 2 study of IMGN901 (lorvotuzumab mertansine; IND# 126953, NSC# 783609) in children with relapsed or refractory Wilms tumor, rhabdomyosarcoma, neuroblastoma, pleuropulmonary blastoma, malignant peripheral nerve sheath tumor (MPNST), and synovial sarcoma: A Children's Oncology Group study. JCO. 2017;35(15_suppl):10537-10537. doi:10.1200/JCO.2017.35.15_suppl.10537

41. Tijink BM, Buter J, Bree R de, Giaccone G, Lang MS, Staab A, Leemans CR, Dongen GAMS van. A Phase I Dose Escalation Study with Anti-CD44v6 Bivatuzumab Mertansine in Patients with Incurable Squamous Cell Carcinoma of the Head and Neck or Esophagus. Clin Cancer Res. 2006;12(20):6064-6072. doi:10.1158/1078-0432.CCR-06-0910

42. Socinski MA, Kaye FJ, Spigel DR, Kudrik FJ, Ponce S, Ellis PM, Majem M, Lorigan P, Gandhi L, Gutierrez ME, Nepert D, Corral J, Ares LP. Phase 1/2 Study of the CD56-Targeting Antibody-Drug Conjugate Lorvotuzumab Mertansine (IMGN901) in Combination With Carboplatin/Etoposide in Small-Cell Lung Cancer Patients With Extensive-Stage Disease. *Clin Lung Cancer*. 2017;18(1):68-76.e2. doi:10.1016/j.cllc.2016.09.002

43. Prota AE, Bargsten K, Diaz JF, Marsh M, Cuevas C, Liniger M, Neuhaus C, Andreu JM, Altmann K-H, Steinmetz MO. A new tubulin-binding site and pharmacophore for microtubule-destabilizing anticancer drugs. *Proc Natl Acad Sci U S A*. 2014;111(38):13817-13821. doi:10.1073/pnas.1408124111

44. Lopus M, Oroudjev E, Wilson L, Wilhelm S, Widdison W, Chari R, Jordan MA. Maytansine and Cellular Metabolites of Antibody-Maytansinoid Conjugates Strongly Suppress Microtubule Dynamics by Binding to Microtubules. *Mol Cancer Ther*. 2010;9(10):2689-2699. doi:10.1158/1535-7163.MCT-10-0644

45. Cassady JM, Chan KK, Floss HG, Leistner E. Recent Developments in the Maytansinoid Antitumor Agents. 2004;52(1):26.

46. Prota AE, Bargsten K, Diaz JF, Marsh M, Cuevas C, Liniger M, Neuhaus C, Andreu JM, Altmann K-H, Steinmetz MO. A new tubulin-binding site and

pharmacophore for microtubule-destabilizing anticancer drugs. *Proc Natl Acad Sci U S A*. 2014;111(38):13817-13821. doi:10.1073/pnas.1408124111

47. Hain KO, Colin DJ, Rastogi S, Allan LA, Clarke PR. Prolonged mitotic arrest induces a caspase-dependent DNA damage response at telomeres that determines cell survival. *Scientific Reports*. 2016;6:26766. doi:10.1038/srep26766

48. Erickson HK, Widdison WC, Mayo MF, Whiteman K, Audette C, Wilhelm SD, Singh R. Tumor Delivery and In Vivo Processing of Disulfide-Linked and Thioether-Linked Antibody−Maytansinoid Conjugates. Bioconjugate Chemistry. 2010;21(1):84-92. doi:10.1021/bc900315y

49. Lu J, Jiang F, Lu A, Zhang G. Linkers Having a Crucial Role in Antibody–Drug Conjugates. *Int J Mol Sci*. 2016;17(4). doi:10.3390/ijms17040561

50. Erickson HK, Park PU, Widdison WC, Kovtun YV, Garrett LM, Hoffman K, Lutz RJ, Goldmacher VS, Blättler WA. Antibody-Maytansinoid Conjugates Are Activated in Targeted Cancer Cells by Lysosomal Degradation and Linker-Dependent Intracellular Processing. *Cancer Res*. 2006;66(8):4426-4433. doi:10.1158/0008-5472.CAN-05-4489

51. Lu J, Jiang F, Lu A, Zhang G. Linkers Having a Crucial Role in Antibody–Drug Conjugates. *International Journal of Molecular Sciences*. 2016;17(4):561. doi:10.3390/ijms17040561

52. Zang X-P, Palwai NR, Lerner MR, Brackett DJ, Pento JT, Harrison RG. Targeting a Methioninase-containing Fusion Protein to Breast Cancer Urokinase Receptors Inhibits Growth and Migration. *Anticancer Res*. 2006;26(3A):1745-1751.

53. Zang X-P, Palwai NR, Lerner MR, Brackett DJ, Pento JT, Harrison RG. Targeting a Methioninase-containing Fusion Protein to Breast Cancer Urokinase Receptors Inhibits Growth and Migration. *Anticancer Res*. 2006;26(3A):1745-1751.

54. Lambert JM. Drug-conjugated monoclonal antibodies for the treatment of cancer. *Current Opinion in Pharmacology*. 2005;5(5):543-549. doi:10.1016/j.coph.2005.04.017

55. Chen L, Wang L, Shion H, Yu C, Yu YQ, Zhu L, Li M, Chen W, Gao K. In-depth structural characterization of Kadcyla® (ado-trastuzumab emtansine) and its biosimilar candidate. *MAbs*. 2016;8(7):1210-1223. doi:10.1080/19420862.2016.1204502

56. Kim MT, Chen Y, Marhoul J, Jacobson F. Statistical modeling of the drug load distribution on trastuzumab emtansine (Kadcyla), a lysine-linked antibody drug conjugate. *Bioconjug Chem*. 2014;25(7):1223-1232. doi:10.1021/bc5000109

57. Wakankar A, Chen Y, Gokarn Y, Jacobson FS. Analytical methods for physicochemical characterization of antibody drug conjugates. *MAbs*. 2011;3(2):161-172. doi:10.4161/mabs.3.2.14960

58. Sun X, Ponte JF, Yoder NC, Laleau R, Coccia J, Lanieri L, Qiu Q, Wu R, Hong E, Bogalhas M, Wang L, Dong L, Setiady Y, Maloney EK, Ab O, Zhang X, Pinkas J, Keating TA, Chari R, Erickson HK, Lambert JM. Effects of Drug–Antibody Ratio on Pharmacokinetics, Biodistribution, Efficacy, and Tolerability of Antibody–Maytansinoid Conjugates. *Bioconjugate Chem*. 2017;28(5):1371-1381. doi:10.1021/acs.bioconjchem.7b00062

59. Peddi PF, Hurvitz SA. Trastuzumab emtansine: the first targeted chemotherapy for treatment of breast cancer. *Future Oncol*. 2013;9(3). doi:10.2217/fon.13.7

60. Goldmacher VS, Blättler WA, Lambert JM, Chari RVJ. Immunotoxins and Antibody-Drug Conjugates for Cancer Treatment. In: Muzykantov V, Torchilin V, eds. *Biomedical Aspects of Drug Targeting*. Boston, MA: Springer US; 2002:291-309. doi:10.1007/978-1-4757-4627-3_15

61. Oroudjev E, Lopus M, Wilson L, Audette C, Provenzano C, Erickson H, Kovtun Y, Chari R, Jordan MA. Maytansinoid-Antibody Conjugates Induce Mitotic Arrest by Suppressing Microtubule Dynamic Instability. *Mol Cancer Ther*. 2010;9(10):2700-2713. doi:10.1158/1535-7163.MCT-10-0645

62. Kovtun YV, Audette CA, Mayo MF, Jones GE, Doherty H, Maloney EK, Erickson HK, Sun X, Wilhelm S, Ab O, Lai KC, Widdison WC, Kellogg B, Johnson H, Pinkas J, Lutz RJ, Singh R, Goldmacher VS, Chari RVJ. Antibody-Maytansinoid Conjugates Designed to Bypass Multidrug Resistance. *Cancer Research*. 2010;70(6):2528-2537. doi:10.1158/0008-5472.CAN-09-3546

63. Ikeda H, Hideshima T, Fulciniti M, Lutz RJ, Yasui H, Okawa Y, Kiziltepe T, Vallet S, Pozzi S, Santo L, Perrone G, Tai Y-T, Cirstea D, Raje NS, Uherek C, Dalken B, Aigner S, Osterroth F, Munshi N, Richardson P, Anderson KC. The Monoclonal Antibody nBT062 Conjugated to Cytotoxic Maytansinoids Has Selective Cytotoxicity Against CD138-Positive Multiple Myeloma Cells In vitro and In vivo. *Clinical Cancer Research*. 2009;15(12):4028-4037. doi:10.1158/1078-0432.CCR-08-2867

64. Hamblett KJ. Effects of Drug Loading on the Antitumor Activity of a Monoclonal Antibody Drug Conjugate. Clinical Cancer Research. 2004;10(20):7063-7070. doi:10.1158/1078-0432.CCR-04-0789

65. Murray N, Salgia R, Fossella FV. Targeted molecules in small cell lung cancer. Seminars in Oncology. 2004;31:106-111. doi:10.1053/j.seminoncol.2003.12.021

66. Tassone P, Gozzini A, Goldmacher V, Shammas MA, Whiteman KR, Carrasco DR, Li C, Allam CK, Venuta S, Anderson KC, Munshi NC. Activity of the Maytansinoid Immunoconjugate huN901-2′-Deacetyl-N-2′-(3-Mercapto-1-Oxopropyl)-Maytansine against CD56 Multiple Myeloma Cells. Cancer Res. 2004;64(13):4629-4636. doi:10.1158/0008-5472.CAN-04-0142

Appendix

72-hr Cytotoxicity Alamar Blue Metabolic Assay

For EMT6, 4T1, and MCF7 Cells

Ben Southard - Revised 2/12/19

Notes: Growth media for EMT6 is Waymouth's Medium (15% FBS, 1% Pen/Strep)

Growth media for 4T1 is RPMI-1640 (10% FBS, 1% Pen/Strep)

Growth media for MCF7 is EMEM (10% FBS, 1% Pen/Strep)

1. In a 96-well plate, seed 5000 EMT6 cells in 200 uL of growth medium per well. Repeat in separate plates for 4T1 and MCF7 cells.
2. A fourth plate will be used for blanks. 5000 cells per 200 uL of the respective growth medium will be seeded in six wells for each of the cell types. 200 uL of each growth medium will also be added without cells into six more wells per cell type.
3. Seeded cells should be incubated for 24 hours at 37ºC and 5% CO_2 in order to recover, adhere, and begin growing.
4. Prepare 150 uL each of 1 pM, 10 pM, 100 pM, 1 nM, 10 nM, 100 nM, 1 uM, 10 uM AV-DM1 conjugate in PBS by serial dilution.

And prepare 150 uL each of 100 pM, 1 nM, 10 nM, 100 nM, 1 uM, 10 uM, 100 uM and 1 mM unconjugated DM1 in PBS by serial dilution.

5. Aspirate and replace the media in all the plates with 180 uL of fresh media.

6. Into each well of the three plates receiving treatment, add 20 uL of each drug in sextuplicute. Incubate all plates for 72 hours at 37ºC and 5% CO_2.

7. Aspirate and replace the media in all the plates with 180 uL of fresh media.

8. Add 20 uL of Alamar Blue to every well of every plate and incubate for 2 hours at 37ºC and 5% CO_2.

9. Read fluorescence: 530 nm excitation, 590 nm emission.

Annexin-DM1 Conjugation

Ben Southard - Revised 2-28-19

1. AV-SMCC preparation

a. Completely dissolve 1.2 milligrams of Sulfo-SMCC in 200 uL of DI water

i. This is a 100x molar ratio to 1 mg/mL annexin, about 10x molar ratio for the available lysine residues on annexin

b. Add all of the Sulfo-SMCC solution to 1 mg of annexin

c. Allow the mixture to react at 4 ºC for 1 hour

2. AV-SMCC purification

a. Dialyze overnight against 2 L of 20 mM phosphate buffer, pH 7.4

i. Membrane MWCO should be between 1 and 10 kDa

3. AV-SMCC-DM1 conjugation

a. Completely dissolve 1.0 milligrams of DM1 in 150 uL of DMSO

i. This is a 50x molar ratio to 1 mg/mL annexin, the degree of Sulfo-SMCC conjugation determines the number of available maleimide reaction sites

b. Add all of the DM1 solution in DMSO to the prepared and dialyzed annexin-SMCC conjugate

c. Allow the mixture to react at 4 ºC for 2 hours.

4. AV-SMCC-DM1 purification

a. Dialyze overnight against 2 L of 20 mM phosphate buffer, pH 7.4

i. Membrane MWCO should be between 1 and 10 kDa

5. Determine the product protein concentration by Bradford assay

a. [(Corrected OD at 595 nm) - .07154] / (.00048) = [protein] in ug/mL

6. Determine the extent of DM1 conjugation by reading absorbance at 288 nm of the conjugate and a blank of unconjugated annexin at the same concentration

a. (Corrected OD at 288 nm) * (.3544) - .0123 = [DM1] in mM